RINGO | Readiness of ICOS

Readiness of ICOS for Necessities of integrated Global Observations

D3.6

Proposition of a roadmap for enhancing ICOS Ecosystem sites to become sentinel sites in cooperation with other domain-specific ESFRI and global infrastructure

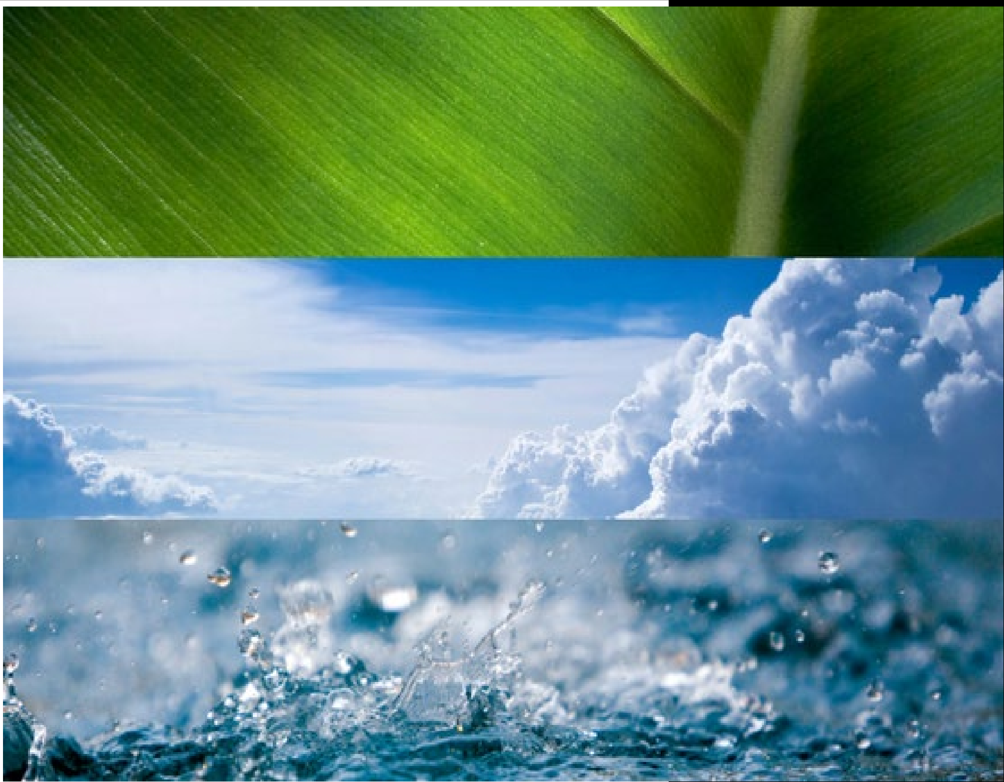

RINGO (GA no 730944)

Public Document/define level

This project has received funding from the European Union's Horizon 2020 research and innovation programme under grant agreement No 730944

Deliverable: Proposition of a roadmap for enhancing ICOS Ecosystem sites to become sentinel sites in cooperation with other domain-specific ESFRI and global infrastructure

Author(s): Virginie Moreaux[1], Gérémy Panthou[2], Béatrice Josse[3], Kevin Lamy[3], Gielen Bert[4], Dario Papale[5], Denis Loustau[1].

Date: 10.12.2020
Activity: RINGO WP3, Task 3.5.
Lead Partner: 3-UNITUS INRA
Document Issue: 1
Dissemination Level: PU
Contact: Denis Loustau (denis.loustau@inrae.fr) (INRAE)

Affiliations: [1]INRAE, UMR ISPA, [2]University Grenoble Alpes, [3]Meteo France CNRS, [4]University of Antwerpen, [5]CMCC and University of Tuscia.

	Name	Partner	Date
From	Denis Loustau	3-UNITUS INRA	25.11.2020
Reviewed by	Elena Saltikoff	ICOS ERIC	04.12.2020
Approved by	Elena Saltikoff	ICOS ERIC	14.12.2020

Version	Date	Comments/Changes	Author/Partner
Final draft	25.11.2020		Denis Loustau
Final version	11.12.2020		Denis Loustau

Deliverable Review Checklist

A list of checkpoints has been created to be ticked off by the Task Leader before finalizing the deliverable. These checkpoints are incorporated into the deliverable template where the Task Leader must tick off the list. [1]

	√
• Appearance is generally appealing and according to the RINGO template. Cover page has been updated according to the Deliverable details.	x
• The executive summary is provided giving a short and to the point description of the deliverable.	x
• All abbreviations are explained in a separate list.	x
• All references are listed in a concise list.	x
• The deliverable clearly identifies all contributions from partners and justifies the resources used.	x
• A full spell check has been executed and is completed.	x

ABSTRACT

The first part of this report is an evaluation of the sensitivity of the Ecosystem station networks to environmental changes that is based upon the FLUXNET2015 dataset recently released. The analysis focused on the impact of environmental changes on ecosystem gross primary production (GPP), as annual integral or instantaneous maximums. We propose a model of ecosystem measurement accounting for the measurement uncertainty, temporal variability and temporal trends. This model allowed us to construct a look up table enabling to estimate the detection sensitivity of large ensemble of network designs, in terms of size, duration and accuracy.

We have applied this model to the FLUXNET2015 dataset analysis. We evidenced the significant temporal trends in GPP with respect to the measurement, partitioning and gapfilling errors as well as the size of the station network and measurement duration. We showed that a temporal trend in GPP may not be detected in time series shorter than 10 years and in PFTs including less than 10 stations.

In a third part of the project, we have been seeking to anticipate the possible future environmental changes that would force European ecosystems for the upcoming 30 years. We used the atmospheric chemistry-transport model CHIMERE made by Météo-France for projecting the temporal changes in key drivers along the 2020-2050 period across Europe at 50 x 50 km resolution. Within the RINGO project, the magnitude of the expected impacts of ozone dry deposition on ecosystems was mapped over Europe allowing us to illustrate the concept of ecozone.

Last, based upon the look-up table of network sensitivity applied to the ecozone concept, we propose a roadmap for optimising the in situ ecosystem observations with respect to the detection and attribution of future environmental impacts.

Table of contents

1. Introduction

- The environmental forcing of terrestrial ecosystems has evolved dramatically for the last 20 years. Since the unprecedented heatwave in 2003, several environmental events were recorded across continents: floodings, droughts, storms, fires, heatwaves. These rare or extreme events are known to affect the functioning of terrestrial ecosystems with immediate or delayed impacts, of which most are lasting for months or even years. More subtle changes in environment are also affecting ecosystems: the background increase in temperature and atmospheric CO_2 concentration, the ratio of diffuse to direct light, pollutants deposition (SOx, NOx, Ox, NHx). From the paradigm of a predictable, steady evolution of climate and atmosphere, these observations lead us to consider the future as largely uncertain with frequent extreme events (storms, heatwaves, droughts) interacting with continuous – but not necessarily monotonous -- drifts in key drivers such as atmospheric state variables (heat and water vapour content, greenhouse gases and aerosols concentrations).

- Across the continents, a number of Research Infrastructures in the Environment domain are observing the temporal and spatial changes in the functioning of terrestrial ecosystems (ICOS-RI, ELTER, NEON, regional Flux tower networks). As far as the ICOS-RI is concerned, the exchanges of greenhouse gases by continental ecosystems are particularly relevant because most of them result from biophysical and physiological processes. In particular, the CO_2 exchanges from vegetated surfaces are actually the “breath” of ecosystems, including both their respiration and metabolic energy intake (Baldocchi, 2008). Their monitoring allows to trace at a half hourly resolution the physiological status of the vegetation, its phenological cycle, nutritional impacts as well as the management effects (Moreaux et al. 2020b). The *in situ* observations addressing simultaneously the measurements of ecosystem biogeochemistry and concurrent changes in the atmosphere, soil, and management have therefore an invaluable role in understanding the responses of the vegetated canopies to the changing environment and to attribute the ecosystem responses observed to drivers.

- The Research infrastructures observing the continental ecosystems must face the complexity of the driving forces at work and their interactions. For most variables observed, the time series of measured values are characterised by the imbrication of temporal and spatial scales, from minutes to decades and from 10^{-6} to 10^{6} m (Baldocchi et al. 2001, Stoy et al. 2005, 2009, Moreaux et al. 2020a). Despite recent and continuous progress in the harmonisation, metrology, and quality of their observations and measurements, the capacity of the network of ecosystem stations to detect the variations of ecosystems functioning and determine their drivers is challenged.

- The detection of the impact of the increase of the atmospheric CO_2 concentration on ecosystem-atmosphere fluxes is well illustrating this challenge. Since the first measurements of atmospheric fluxes of CO_2 by the eddy covariance technique (Wofsy et al. 1993), the atmospheric CO_2 concentration observed has increased from 357 to 415 ppm in the northern hemisphere. Such an enhancement would influence the CO_2 assimilation by plant canopies significantly but several attempts to evidence such an impact in the time series of CO_2 flux measured over one or several station values were not clearly conclusive (Fernandez-Martinez et al. 2017). Only consistent and long time series from stations with low inter-annual variability suggest such an effect (Pilegaard et al. 2011, Horemans et al. 2020). Baldocchi et al. (2018) demonstrated that, given the error in measurements, the duration of the time series is indeed a key factor for the detection.

- For optimising the capacity of in situ networks of stations to detect temporal and spatial changes, there is indeed a critical need of a general framework that could apply to the real world. Such an analysis would also provide tools for optimising network of stations in terms of network size, station location, monitoring duration and to identify target variables measured and their accuracy.
- Within the framework of the RINGO task 3.5, we have established a simple model of ecosystem measurements and used this model to assess the detection sensitivity of networks of ecosystem stations of varying size, accuracy and duration. First, we reviewed the components of the errors of a key variable determined from ecosystem measurements, the gross carbon assimilation or gross primary productivity (GPP). We used then a MonteCarlo technique and trend analysis for investigating how the network size, duration and accuracy are conditioning its detection capacity. We used the model to estimate the marginal gain of improving the network size, duration and measurements accuracy for detecting a change in ecosystem atmospheric exchanges.
- The recent release of a large ensemble of eddy covariance datasets offers an opportunity to apply the model for the case of a stations network. The FLUXNET-2015 data set includes stations having monitored atmospheric fluxes at the continental levels for continuous periods extending from 4 to 21 years. Their data were processed homogeneously using several options and measurements uncertainty was determined (Pastorello et al. 2020). This ensemble can be used for calculating measurement uncertainty, accuracy, temporal variability and long-term trends and split this calculation among several Plant Functional Types. Here, the FLUXNET2015 data set was used to test the capacity of historical network of ecosystem stations to detect changes in CO_2 assimilation (gross primary production, GPP). We analysed the temporal changes of the annual sum and instantaneous maximal value of GPP, and quantified its temporal variability and uncertainty.
- We further developed the temporal analysis of ecosystem measurements using homogenised 8 year-long time series of five ecosystem stations in France, where the correlation patterns and temporal spectrum of key ecosystem variables for different PFTs were investigated using power spectra and Random Forest analysis. The results and conclusions have been published and are therefore not detailed in this report (Moreaux et al. 2020b).
- Last, in order to illustrate how the ecosystem network might be design and optimised, we projected the expected ozone deposition on the ecosystem stations composing the ICOS Ecosystem network for the next 30 years. From this analysis, we proposed to optimise the ecosystem observations for enabling them to detect and attribute the future changes to its drivers.

2. Uncertainty linked to the EC methodology. The single station case.

The eddy covariance (EC) method is used in the ICOS-RI, ELTER, NEON and by the regional networks of stations across the world to calculate vertical turbulent fluxes of momentum, energy and gases exchanged between the continental surface and the atmosphere (Baldocchi 2014). The EC method and the instruments used for are prone to a number of limitations which are sources of errors in the data measured. In addition, starting from the same raw data set, different processing schemes of flux computation may produce a 5 to 10% difference in final values (Mauder et al. 2008). Also, simultaneous raw data sets obtained from different sensors operating in the same site can result in a 10 to 15% difference (Mauder and Foken, 2006, Mauder et al. 2008, Goodrich et al. 2016).

We consider more specifically two sources of error (Moncrieff et al. 1996): systematic errors (frequency response errors, physical consideration, Instrument calibration, gas flux storage, u* filtering) and random errors (Instrumental noise, stochastic nature of turbulence (Wesely and Hart, 1985) and footprint inhomogeneity). Considering an optimal measurement setup with well calibrated sensors (Rebmann et al. 2018) and a standardised scheme of data processing, we can assume that the systematic measurement error is minimised. The random error of the fluxes is thus dominating the EC flux measurement uncertainty at short timescales. It refers to the stochastic nature of turbulence, i.e. the sampling error expressed by the flux error of the covariance (Finkelstein and Sims, 2001, Salesky et al. 2012) and the error due to the instrumental noise (Lenschow et al. 2000, Billesbach 2011).

The total random uncertainty associated with each 30 min span represents the standard deviation of the covariance of the scalar and the vertical wind speed component. The covariance can be evaluated according to Finkelstein and Sims (2001) with a statistical approach, the one-point sampling error approach. A daily differencing approach or self-differential approach is also commonly used (e.g. in FLUXNET2015 dataset) (Hollinger and Richardson, 2005, Richardson et al. 2006).

The other major source of error in the flux data is due to the filling of gaps in data time series. The quality control of the 10 Hz frequency data leads to reject a substantial fraction of data, spikes and outliers, when turbulence drops below a given threshold (u* threshold) or not passing the stationary test. The uncertainty in the friction velocity, u*, threshold estimate represents one of the largest components (Wutzler et al. 2018) because the higher is the u* threshold, the larger is the amount of half-hourly data discarded, increasing the amount of data to gap-fill and associated uncertainty.

For filling the gaps in the time series let by data rejection (QA/QC tests, Mauder and Foken 2006 and u* threshold, Papale et al. 2006), different procedures are used: statistical interpolation, neural-network, parametric, or mechanistic models (Reichstein et al. 2005, Falge et al., 2001). The related uncertainty is within the same order of magnitude than the measurement random uncertainty (Wang et al. 2015). We illustrated these two sources of errors for the FR-Pue time series 2001-2014, an Evergreen Broadleaf Forest ecosystem (EBF). Our results (fig. 1) confirm this conclusion, the “gapfilling” uncertainty being even larger than the random uncertainty.

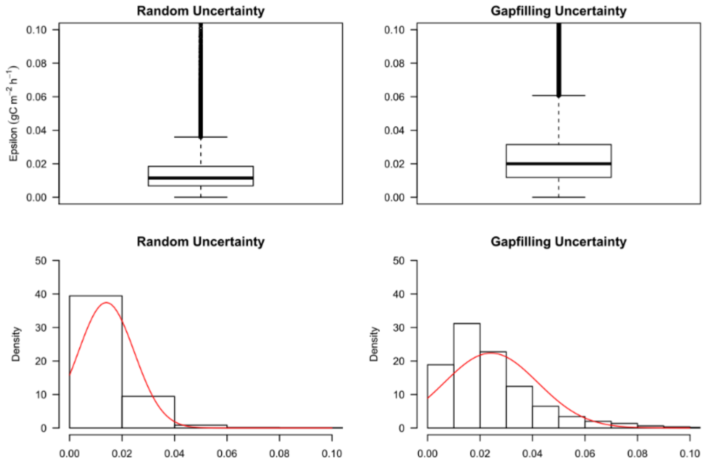

Figure 1. Example of uncertainty assessment for FR-Pue (mediterranean EBF) over the period 2001-2014. Random uncertainty is computed from Finkelstein and Sims (2001), the gap-filling uncertainty is provided by Reichstein et al. (2005).

1.1 Error propagation

We explore the error propagation of flux uncertainty over the period 1995-2015 based on gapfilled time series of half hourly data and across a range of integration durations. Within the RINGO Task 3.5 we have first used the data from the FLUXNET2015 database for 31 ecosystem European stations which represents a pre ICOS ecosystem network. We calculated a joint uncertainty, ε, as the combination of random uncertainty (Richardson et al. 2006) and the gap-filling uncertainty (u* filtering uncertainty). Since random errors accumulate "in quadrature", ε was calculated as $\sqrt{\varepsilon_1^2 + \varepsilon_2^2})$ where ε_1 and ε_2 are measurement and gap-filling errors respectively. In accordance with previous studies, we showed that the uncertainty is negligible at the 30min time step (Figure 2), that is the averaging period of the EC flux computations. Due to gap filling error, the joint uncertainty of the CO_2 flux integrals increases with the integration time, reaching a mean value among stations of 27.3 gC m^{-2} for yearly integrals (n = 31 sites, min: 6.93 gC m^{-2}, max:165 gC m^{-2}).

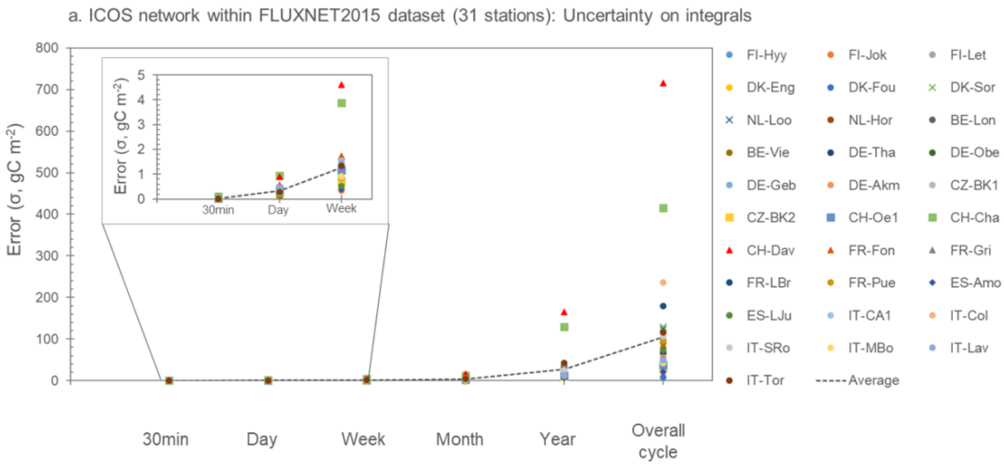

Figure 2. Error propagation on CO_2 flux in terms of total uncertainty (random + gap-filling) from 31 stations of the FLUXNET2015 dataset (Richardson et al. 2006 + ustar filtering).

1.2 Statistical power of EC studies

Recent studies started to consider the spatial and temporal performance of a network within the context of detectable changes. Hill et al. (2017) has recently estimated the number of replications needed for a robust flux computation for one station. They defined the effect size by the magnitude of the difference in mean fluxes from two towers, relative to the total measurement uncertainty. In this study, the uncertainty was assessed using a self-referential approach (Richardson et al., 2006). However, spatially replication of EC system in the same station is a challenge, especially due to high equipment costs.

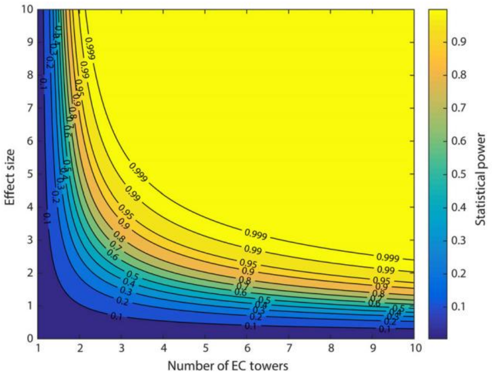

Figure 3. From Hill et al. (2017), Statistical power, that is the probability of correctly rejecting the null hypothesis (no difference between two ecosystems) , H0, as a function of the effect size and the number of eddy covariance towers per ecosystem. The effect size is taken to be Cohen's d.

Hill et al. showed that for a typical ecosystem, around four EC towers are needed to have 95% statistical confidence that the annual flux of an ecosystem is nonzero. Furthermore, if the true flux is small relative to instrument noise and spatial variability, the number of towers needed can rise dramatically.

Shao et al. (2015) underlined the duration of a time series needed for detecting temporal trends. Recently, using a Monte-Carlo simulation to derive the detectable thresholds for trends and interannual variability of the annual carbon fluxes, Baldocchi et al. (2018) have estimated the duration needed for detecting a step change and a temporal linear trend in the time series of NEE measurements. For instance, the fig. 4 shows that, given a measurement error of 30 gC m^{-2} y^{-1}, the monitoring duration should exceed 8 years for detecting a trend of interannual NEE reaching 7 gC m^{-2} y^{-2}. If the data records exceed 20 years, trends as small as 3 gC m^{-2} y^{-2} can be detected whatever is the uncertainty (i.e., ± 10, ± 30, or ± 60 g C m^{-2} y^{-1}) (Figure 4).

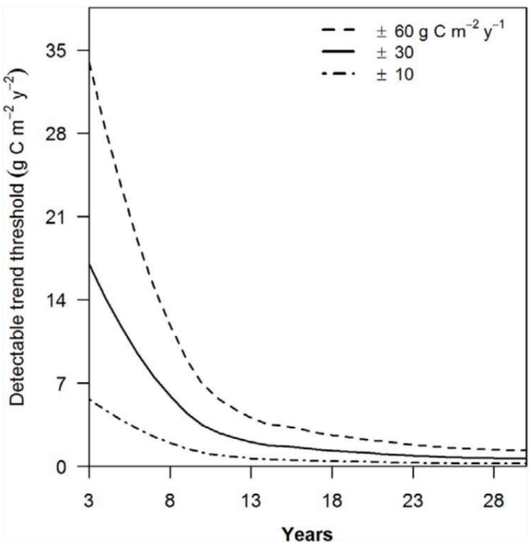

Figure 4. From Baldocchi et al. (2018). confidence intervals of the detectable tr random time series of varying lengtl uncertainty.

3. Detection capacity of a virtual network of Ecosystem stations

3.1 A general model of ecosystem measurements

We model the measured value of an ecosystem variable measured by a network of *in situ* stations as the random variable:

$$X_{t,\ j} = 1 + t \times a \ \pm \acute{\alpha} \qquad \text{(Eq.1)}$$

where $X_{t,\ j}$ stands for the normalized variable value (e.g. GPP) at time *t* and in station *j*, parameter *a* refers to the slope, *i.e.* the linear change in the variable attributed to a change in an environmental parameter (e.g. atmospheric CO_2 increase, temperature, air vapour pressure saturation deficit etc.) and $\pm\acute{\alpha}$ for the detrended temporal variability of the variable X. The latter is the sum of the measurement uncertainty, ε, as discussed in the previous section, and the "natural" residual variability, σ, caused by temporal changes in external drivers or endogenic processes, so that $\acute{\alpha} = \varepsilon + \sigma$.

Actually, the equation (1) extends the statistical analysis developed in Baldocchi et al. (2018). We assume further that the stations measuring X within the same environmental area and on the same Plant Functional Type may be treated as independent replicates. We can therefore enrich the analysis previously developed by Baldocchi et al. (2018) including the number of stations considered and the decomposition of the overall temporal variability of X, among three components:

- a linear drift, *a*,
- an error term, ε,
- the natural detrended temporal variability, σ.

The calibrations of *a*, ε and σ using the FLUXNET2015 dataset are further described in section 4.

3.2 Network experiment - method

For assessing the sensitivity of a network of stations, we created a virtual, ideal, network composed of similar stations in ecosystems belonging to the same PFT. The distribution of the error term, ε, and variability, α, were calibrated from legacy data of the FLUXNET2015 dataset as explained in section 4. Different network designs in terms of station numbers (1 to 70), error (0.02 to 0.18), and measurement duration (3 to 25 years) were generated. An ensemble of datasets measured by each network design was simulated by Monte Carlo approach (*n* = 5000) using the models of distribution of error, ε, and variability, σ, fitted on the FLUXNET2015 time series of GPP, i.e. a Normal and Gamma distributions respectively. The parameters distribution was assumed constant in time. The experiment is summarised in Table 1.

For each of the 5000 generated samples of each network design (27 × 70 × 56), a linear regression on time was fitted and the Student's t value on slope calculated. A network having more than 95% probability (>4750) of concluding to a significant slope of X over time is considered as able to detect the trend. Conversely, when the linear regression slope was significant in less than 95% of samples, the network was considered as unable to detect the trend. The statistical analyses were performed with SAS 9.4 Statistical Software Package (SAS Institute, Cary, NC, USA). The ensemble of results is a look-up table providing the sensitivity of all possible (n = 105 840) network configurations.

Table 1. Simulation plan

Variables and parameters	Start	End	by	Runs
Time unit: (*t*)	3	30	1	27
Station (*j*)	1	70	1	70
Error (ε)	5%	60%	1%	56
Slope (*a*)	0.50%	2%	0.1%	16
Monte Carlo (*k*)	1	5000	1	5000

3.3 Network experiment – results

For illustrating the potential interest of this experiment, the fig. 11 summarises the results obtained for four values of temporal trend, a = 0.005; 0.010, 0.015, 0.02 yr^{-1}. In each graph, the three axis represent the network size (x), temporal variability (y) and duration (z), respectively. Each point of the blue gridded surface is the minimal duration for which the regression of X on time was significant in >95% of the 5000 runs. The temporal trends that are below the surface are not detected with p=0.95 confidence. Hence, the surface sets the detection threshold or sensitivity of the station networks. The red dotted lines correspond to the case of a network of stations corresponding approximately to the size (n = 10) and temporal variability of the FLUXNET2015 ENF stations (ε = 0.07, σ = 0.19, α = 0.20). The lower is the surface within the plot, the more sensitive is the network. The fraction of the 3D volume above the surface may be seen as the detection capacity of the station networks while the corresponding value below the surface represents the "blind" network designs.

In the example in fig. 5, the network ENF size and variability are shown as red lines. The network may detect a 0.005 trend after 30 years, a 0.01 trend after 18years and a 0.002 trend after10 years. This is consistent with results shown in section 4 where the ENF stations of the FLUXNET2015 dataset evidenced a temporal trend of 0.15 to 0.28 within a 10-year time. The profiles of the detection surface along the three axis indicates the gain in sensitivity expected when increasing the network duration (z vertical axis), network size (x horizontal axis) or temporal variability (y horizontal axis). The gain is larger when the profile is steeper.

The model experiment shows that the sensitivity gain does not increase linearly with size, duration or temporal variability, $\acute{\alpha}$: maximal gains are observed from a size of 1 to 12 stations and a duration from 0 to 15 years. Increasing the number of stations is thus critical for detecting changes but adding supplementary stations beyond n = 10 adds little gain in sensitivity. The temporal variability has a negative effect on the detection threshold. This effect is approximately linear but with a steeper slope for small values of *a*. It means that the gain expected from reducing the temporal variability of measurements is larger for the detection of small temporal trends (<0.02 y^{-1}), such as the CO_2 effect on GPP.

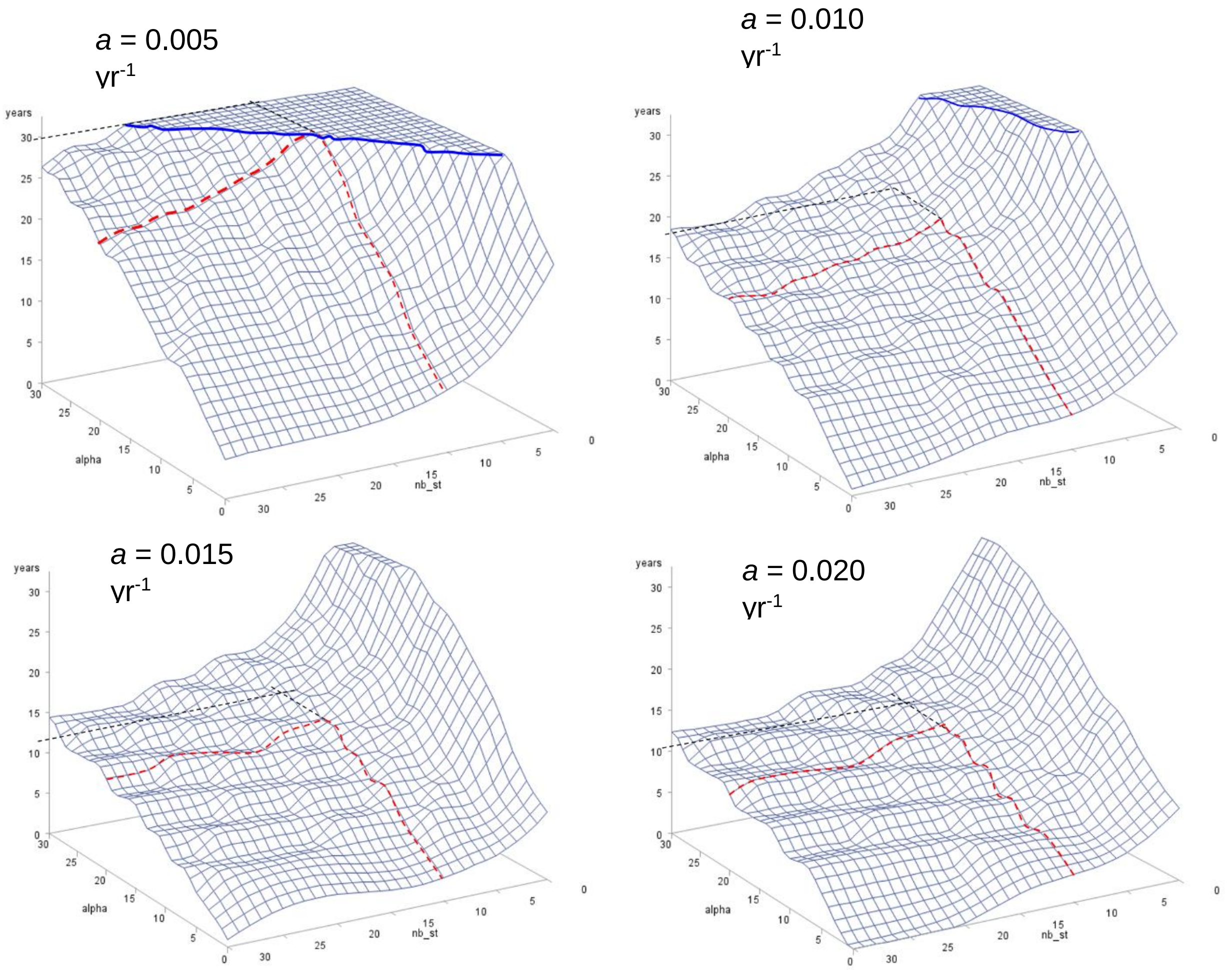

Figure 5. Surface of detection for four temporal trends (*a* = 0.5% , 1%, 1.5% and 2.0% yr^{-1}). The *x*-axis represents the number of stations in the network (from 1 to 30), *y*-axis is the temporal variability α (from 0% to 30%) and z-axis the duration of the network (0 to 30 years). The red lines illustrates the case of network of 10 stations with a variable showing a variability of 20% such as the ENF type in the FLUXNET2015 database. Projection on the time axis (black dotted line) shows that detection time decreases from 30 to 10 years when a increases from 0.5 to 2% year^{-1}. The blue line at the top of plot is the detection limit.

4. Reanalysis the Fluxnet 2015 dataset time series. The network of stations case

In order to quantify the capacity of a network of stations to detect temporal changes, we have assessed the potential of EC towers network to a change in gross primary production, GPP. We applied the concept previously developed for modelling the variable values measured from ecosystem stations to the case of the annual GPP as determined by historical stations included in the FLUXNET2015 dataset. We used the FLUXNET2015 database to assess the error and interannual variability of historical stations.

4.1. Target variable.

The variable GPP was selected because it reflects the photosynthesis of the canopy foliage whose determinism is well understood and documented for most plant species and canopies. The terrestrial GPP is controlled by the amount of light absorbed by the canopy, the CO_2 concentration at internal carboxylation sites, and metabolic carboxylation capacity of the canopy. The GPP is therefore expected to respond to the main environmental forcings: climate, water cycle, CO_2 concentration, pollutants deposition.

GPP is not measured by ecosystem stations but calculated from the net flux of CO_2 exchanged, NEE. The latter can be partitioned into two components, the ecosystem respiration and photosynthesis, based on the fact that photosynthesis is null during night. The Lasslop et al. (2010) partitioning method was used. We selected two time integrals of the photosynthetic CO_2 assimilation, GPP, the annual sum, or GPP (gC m^{-2} y^{-1}), and its half hourly annual maximum, thereafter GPP_{max} (µmol CO_2 m^{-2} s^{-1}). The former was chosen because integrating a whole growing season and the latter because the CO_2 effect on photosynthesis is larger under light saturated conditions, when the Leaf Area Index (LAI) is maximal and plant stomata fully open, e.g. at high air humidity and on wet soil. Moreover, the gap-filling error is null for GPP_{max} that is prone to the only random uncertainty. In order to minimise the latter, we calculated GPP_{max} values as the average of the *n* values in the upper quartile of half-hourly GPP determined in June, at VPD <1600 Pa on wet soil and under a downward photosynthetic photon flux density PPFD > 1400 µmol m^{-2} s^{-1} or shortwave radiation flux density >700 W m^{-2}. The random error on GPP_{max} is thus reduced by a factor $1/\sqrt{n}$.

Among other forcings, the control of the photosynthesis in C3 plants by the atmospheric concentration of CO_2 is well known. However, the GPP effect of CO_2 interacts with, e.g., plant nutrition, water availability or temperature which makes the only CO_2 effect difficult to detect and quantify (Zaehle et al. 2014). In order to assess the effect of the historical enhancement in CO_2 concentration and the corresponding temporal trend of GPP and GPP_{max} to be expected we simulate the corresponding temporal trend using the forest model GO+ that is a simple process based model of forest functioning, production and growth (Moreaux et a. 2020a). The model can be applied to various species (Eucalypt, Douglas fir, Coffee, European Beech, maritime Pine, Oaks) and management schemes (standard, coppice, agroforestry). In this exercise, GO+ was parameterized for a temperate evergreen needleleaf forest (FR-LBr in the FLUXNET2015 database) where the model simulates the canopy growth and LAI satisfactorily. Two runs were considered:

- Run1 “control”: CO_2 concentration was fixed at a value of 343 ppm from 1984 to 2011.
- Run2 ”historical”: CO_2 concentration is the historical record on site and grows from 343 ppm in 1984 to 390 ppm by 2011.

Comparing the outputs of the two simulations, we found that the CO_2 anomaly reached 170 gC m^{-2} y^{-1} in 2008. This represents a linear drift of (+ 6.8 gC m^{-2} y^{-1}) y^{-1} over the 1984-2008 period, i. e +0.50% y^{-1} (Fig. 6). The question raised is then how much is the uncertainty on the target variables used, GPP and GPP_{max}.

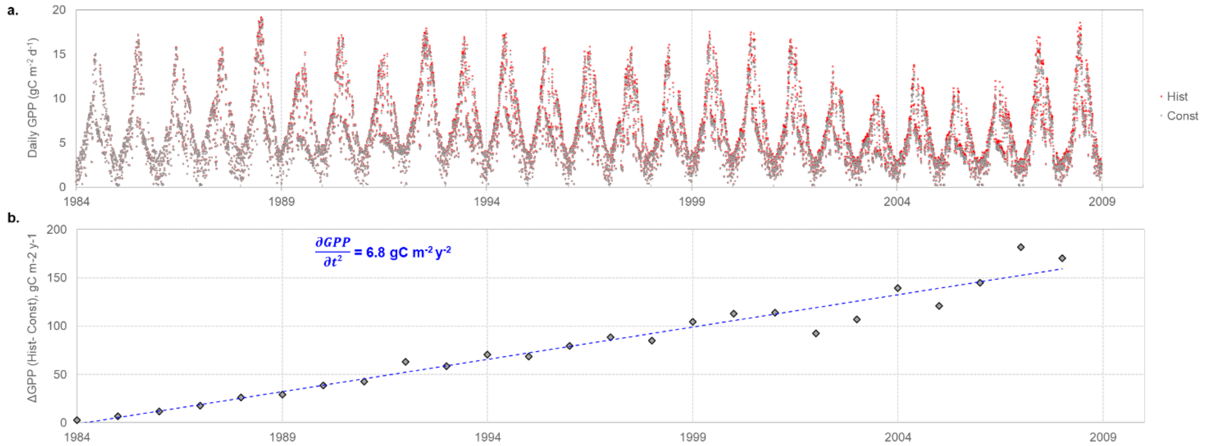

Figure 6. Daily GPP over 1984-2010 simulated by the GO+ model at constant (grey) and historical CO_2 concentrations (red) at the FR-LBr ENF forest in Southwest of France (a). The CO_2 anomaly on GPP over the 1984-2008 period and its regression on time are plot in the lower diagram (b).

4.2. Uncertainty and inter-annual variability of target variables calculated from the FLUXNET2015[1] data set.

4.2.1. Preliminary analysis of the annual values of GPP.

The annual FLUXNET2015 dataset includes 206 sites providing annual values of GPP, equivalent to 1181 site-years (stations list in appendix 1). For one station j, annual GPP was first decomposed as follows:

$$GPP_j = \overline{GPP_j} \pm \alpha_{GPP,j} \qquad \text{(Eq. 2)}$$

where $\overline{GPP_j}$ is the average of annual values of GPP that is 'GPP_NT_CUT_REF' of station *j* in the FLUXNET2015 database and $\pm\alpha_{GPP,j}$ is its bulk, undetrended, standard deviation (Figs 7-8). When combining the 147 sites, we obtained an average value of GPP = 1243 gC m^{-2} and an average standard deviation α_{GPP} = 261 gC m^{-2}, which corresponds to 21% of GPP. We also found the distribution of the standard deviation of GPP is well fitted by a gamma law which will be used further more for modelling the ecosystem GPP measurement (fig. 8).

[1] (ex. FLX_ IT-Col _FLUXNET2015_FULLSET_YY_1996-2014_1-3.csv) provided through the portal http://fluxnet.fluxdata.org/

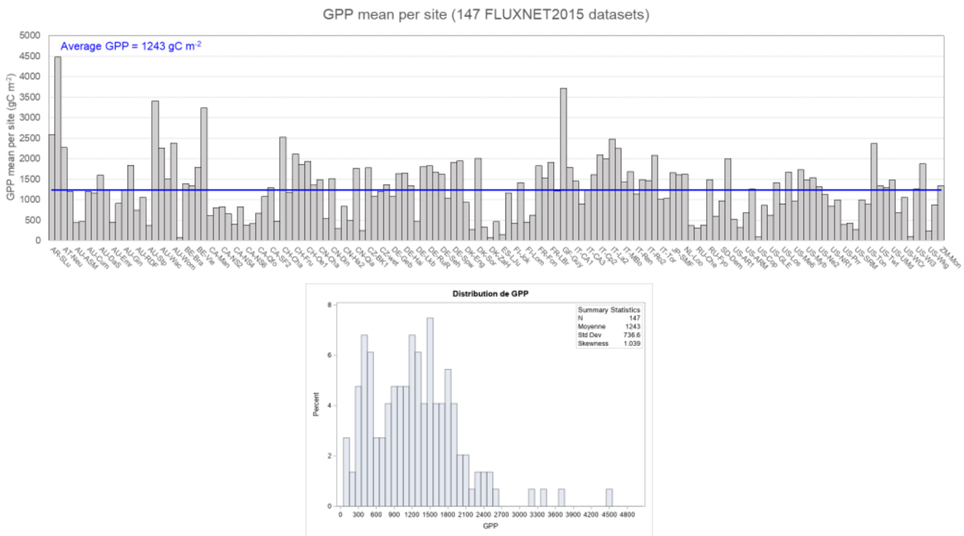

Figure 7. Average of the annual GPP per site (upper graph, units are gC m^{-2} y^{-1}) and histogram of the distribution (bins=100) (lower graph).

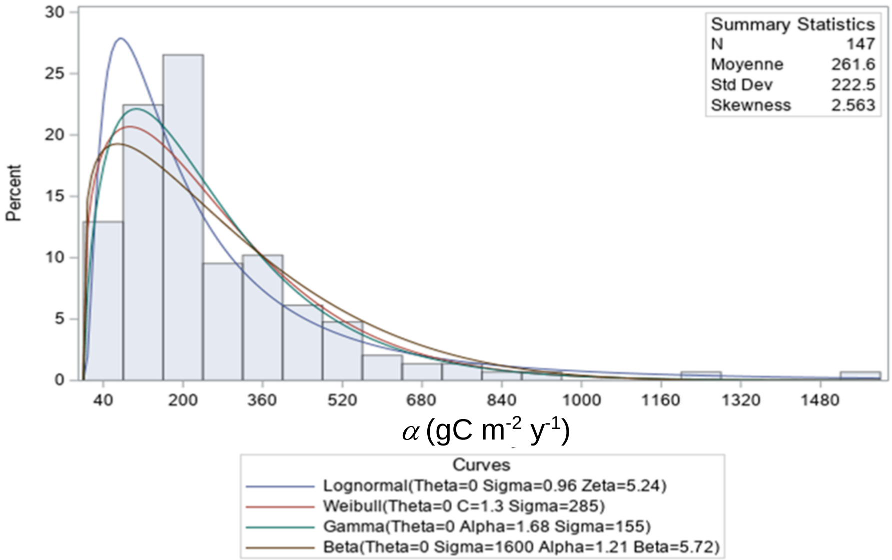

Figure 8. Frequency distribution of the standard deviation of annual GPP, α. Models adjusted with their respective parameters are given in the legend.

4.2.2 Calibration of measurement model

Linear trend and detrended overall variability

For calibrating the general model of ecosystem measurement (Eq. 1), the same processing was used for both GPP and GPP_{max}. The 4 year-, 10 year- and 21 year- long time series of GPP and GPP_{max} were first regressed over time and the linear slope, the parameter *a* of the model, was estimated. The standard deviation of the detrended time series, parameter $\acute{\alpha}$, was then calculated -but not yet partitioned into random uncertainty and natural variability at this stage-. The figure 9 illustrates the results obtained over 10 year-long time series. The corresponding figures of the 4 year- and 21 year-long time series are in appendix 2 fig. A2. The PFTs having the largest number of stations, the crops (CRO, 9 stations) and evergreen needleleaf forests (ENF, 13 stations) showed a significant ($p<0.05$) linear trend over time. While the ENF slope was positive (+0.015 y^{-1}), the temporal trend of crop GPP was negative (-0.03 y^{-1}) due to extremely low values in 2013. The grasslands stations (n=4) showed also a significant positive trend with p value = 0.1. Though not significant, the same trends were revealed in 4 year-long time series. Only one site, the Harvard forest, could be analysed over a 21 year-long series of annual GPP that showed a significant, positive, trend (+0.01 y^{-1}).

The analysis on GPP_{max} led to similar conclusions than GPP. The list of sites involved is in appendix 3. The error on GPP_{max} was calculated for the two main methods of partitioning and gap filling, abbreviated as NT for night-time (Reichstein et al. 2005) and DT for day-time (Lasslop et al. 2010). Both led to similar results and only the latter, DT, is shown here (fig. A3 in appendix 4). The random uncertainty was entirely due to measurement errors since no gap filling was applied. The temporal trends of the 10 year-long time series are shown in fig. 9 and corresponding figures for the 4 year-long and 18 year-long time series are in appendix 5 (fig. A4). On average, the temporal variability of GPP_{max} was higher than GPP, that is clear in crops (CRO) and coniferous forests (ENF). The 10 year-long time series showed a significant positive trend of GPP_{max} for the only ENF (+0.028 y^{-1}). The mixed forest (MF) exhibited also a positive temporal trend (+0.015 y^{-1}) with p value close from 0.10. The crops did not show a significant temporal trend. The number of replicates is higher for the ENF type and may explain why the regression over time was significant in this case and not for other PFT with less replicates. The results also demonstrate that the monitoring duration plays a key role in evidencing temporal trends. Although generally higher, the positive trends in GPP and GPP_{max} detected in coniferous, grasslands and mixed forests are in the order of magnitude of the expected effect of CO_2 increase on GPP and GPP_{max}.

Random uncertainty

The FLUXNET2015 database provides the opportunity to assess the random uncertainty component on GPP and the Ecosystem Respiration (Reco) across sites. Indeed, this is the first database combining different sources of uncertainties and providing a unique variable, called the JOINT UNCERTAINTY, which includes the random uncertainty and the u* filtering uncertainty.

The joint uncertainty was assessed for the variable NEE_CUT_REF. The random uncertainty in the measurements is estimated on the half hourly data and quadratically summed for the other time scales. The methodology used for estimating the random uncertainty is based on Richardson et al. (2006). This self-differential approach requires measured values with similar meteorological conditions within a given sliding window of ± 7 days and ± 1 hour of the current timestamp. The random uncertainty, RANDUNC, is calculated as the standard deviation of the measured fluxes within a given window. The meteorological conditions criteria are air temperature within ±2.5 °C, vapour pressure deficit within ±5 hPa and incoming shortwave radiation ±50 W m^{-2} when higher than 50 W m^{-2} or ±20 W m^{-2} otherwise.

Gap filling error

The gap filling error is produced by the gap gilling method used, here the marginal distribution sampling (Reichstein et al. 2005). Its magnitude is linked to the u* threshold selected. The u* threshold is estimated in the FLUXNET2015 data set by the *Moving Point Test* according to Papale et al. (2006) and the estimation of uncertainty of the threshold is processed by bootstrapping the data within a year.

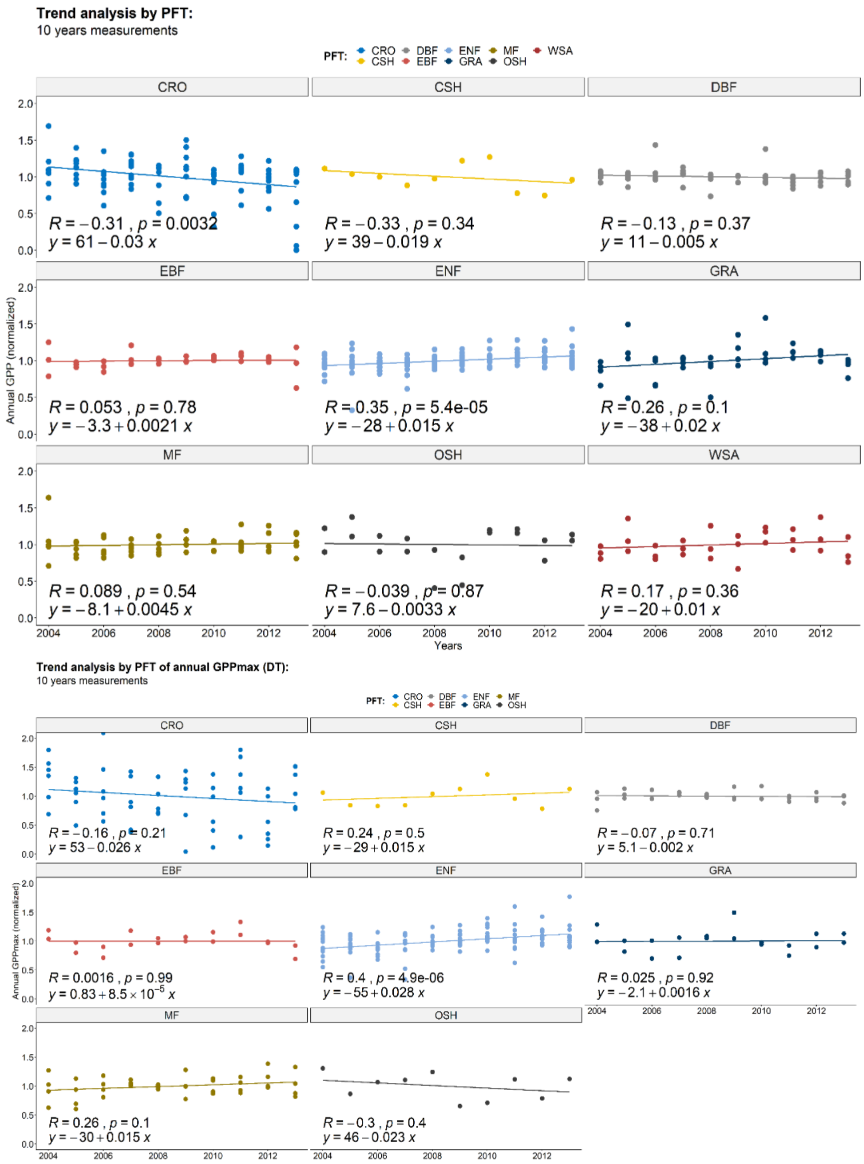

Figure 9. Linear regression of GPP (above diagrams) and GPP_{max} (below diagrams) over time by PFT along 10 year-long time series.

Resulting cumulated error

Since GPP is calculated using values measured at night and during the day (Lasslop et al. 2010), we considered that the uncertainty in hourly values of GPP at station *j* is the quadratic sum of the error in nightime and daytime error values:

$$\varepsilon_{GPP,j} = \sqrt{\bar{\varepsilon}^2_{NEE,j,Night} + \bar{\varepsilon}^2_{NEE,j,Day}} \qquad \text{(Eq. 3)}$$

When averaged over n stations of the PFT *P,* the error components are the average over the *n* stations of the PFTs:

$$\bar{\varepsilon}_{NEE,P,NT} = \frac{1}{n} \times \sum_{i=1}^{n} \left(\frac{NEE\_CUT\_REF\_NIGHT\_JOINTUNC}{NEE\_CUT\_REF\_NIGHT} \times 100\right) \qquad \text{(Eq. 4)}$$

$$\bar{\varepsilon}_{NEE,P,DT} = \frac{1}{n} \times \sum_{i=1}^{n} \left(\frac{NEE\_CUT\_REF\_DAY\_JOINTUNC}{NEE\_CUT\_REF\_DAY} \times 100\right) \qquad \text{(Eq. 5)}$$

The error on the integral over a time series of *t* values is therefore :

$$\bar{\varepsilon}_{GPP,P} = \sqrt{t} \times \sqrt{\bar{\varepsilon}^2_{NEE,PFT,Night} + \bar{\varepsilon}^2_{NEE,PFT,Day}} \qquad \text{(Eq. 6)}$$

The detrended variability of GPP, $\acute{\alpha}$, was calculated accounting for the linear trends detected, whatever their statistical significance (Fig. 10). Apart from the crops, the variability varies among PFT between 10 and 20% and shows no systematic trend with respect to the duration of the time series considered. The GPP variations are weaker in deciduous broadleaf forest type and almost even among other types. Finally, knowing the random uncertainty, $\bar{\varepsilon}_{GPP,P}$, , and the overall detrended variability, $\acute{\alpha}$, the residual natural variability, $\bar{\sigma}_{GPP,P}$, can be calculated as well.

The uncertainty calculation and Eq. 3 to 6 could be resolved for 147 sites and the results obtained are provided Fig. 10 and Table 2. Since the error term ε tends to cancel out when integrated over large time series, the error on annual GPP is three order of magnitude less than the temporal variability, $\acute{\alpha}$, (Table 2).

The results obtained show that once excluded PFT with less than 2 stations the following conclusions may be drawn:

- the random “measurement” uncertainty on annual GPP, ε, is negligible;
- the crops show the largest temporal variability, presumably due to the changing practices from year to year (crop rotation, soil preparation, fertilisation, residues management).
- the forests (DBF, EBF, ENF, MF) tend to show less variability than crops, shrublands and grasslands and their inter-annual variability is in the range of 9 to14%.

These observations should not be over interpreted owing to the small size and uneven representativeness of the samples selected. The higher variability of annual GPP may be due to multiple factors such as climate, management practices, pollution and some PFTs, e.g., the coniferous stands, covers a wider range of climate than other types. Nevertheless, this analysis provides a synthetic, cross PFT’s comparison of the errors recorded in historical time series available.

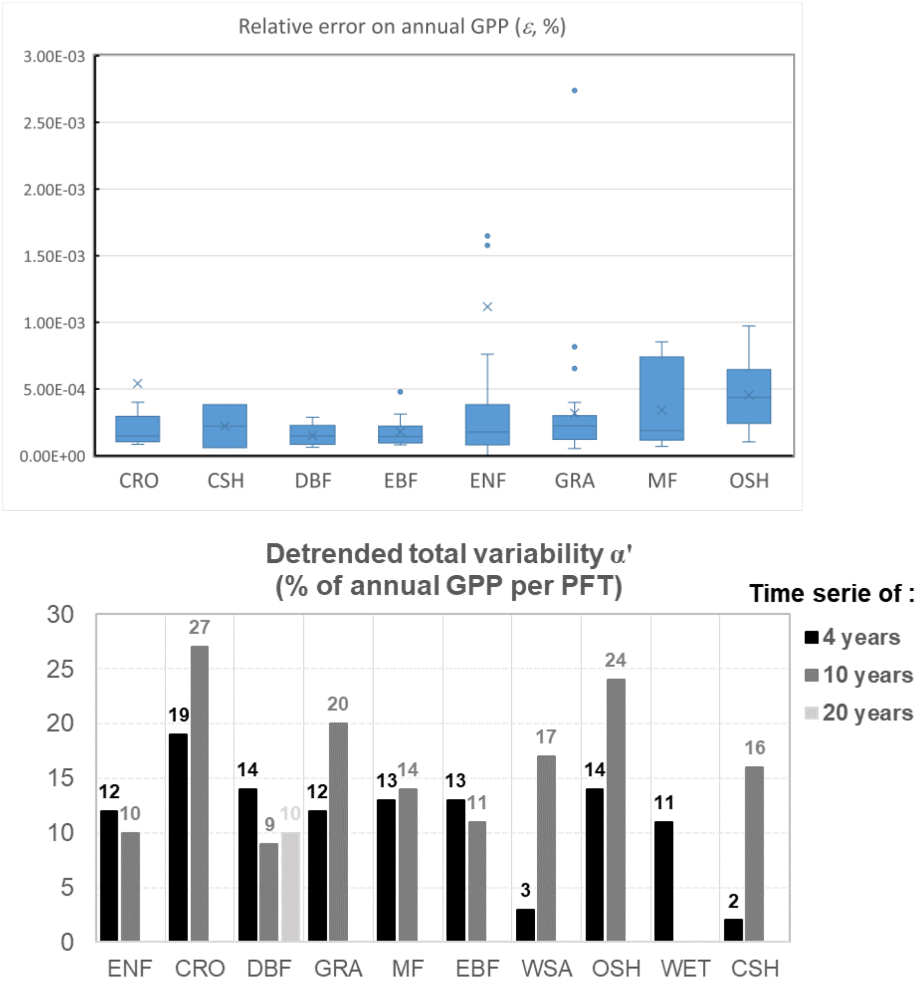

Figure 10. Error on mean annual GPP, $\bar{\varepsilon}_{GPP,P}$, estimated from Eq. (6) (top diagram) and detrended inter annual variability of GPP, $\acute{\alpha}$, for 8 PFTs and three time series durations (below diagram).

Table 2. Normalised values of error components on GPP split by Plant Functional Type and calculated using the FLUXNET2015 dataset for 10 year-long time series, n is the number of stations included.

	CRO	CSH	OSH	DBF	EBF	ENF	MF	GRA	WET	WSA
σ	0.25	0.09	0.26	0.15	0.14	0.19	0.19	0.18	0.29	0.18
ε (E-3)	0.54	0.22	0.45	0.15	0.18	1.14	0.34	0.31	0.17	0.33
n	7	1	2	5	3	7	5	4	1	1

5. Application to the ecosystem network optimization for 2020-2050

5.1 Application of the European continental area.

Here, we enlarge the previous approach to the entire continental European area surface. For extrapolating our model at the European level we assume the following:

- the environmental forcing regime for the upcoming 30 years is spatially homogenous over spatial domains;
- the effect of the drivers considered on ecosystem of the same PFT can be assumed similar among stations in terms of temporal change and magnitude;
- the European continental area can be simplified as the juxtaposition of several conterminous areas within which the above assumptions are satisfied.

We call these homogenous areas “ecozones”. The ecosystem stations monitoring the same PFTs within the same ecozone could thus be considered as replicates. The ecozone concept is flexible and can be adapted to the drivers considered, i.e. ecozones may vary in relation to the driver, management and ecosystem considered.

For analysing the capacity of the ICOS Ecosystem network to evidence the future impacts of environmental changes on the ecosystem-atmosphere exchanges across Europe, we propose therefore to clustering the ecosystem stations in subgroups where temporal evolution of the forcing variables and ecosystem response can be considered as approximately homogenous. We need therefore to assess the expected environmental changes for the next 30 years across Europe for providing a prior map of the main European ecozones, as proposed in the following section 5.2.

The look-up table constructed from the virtual network experiment above will then allow us to determine the best minimal network configuration requested for detecting environmental impacts within and across ecozones. For convenience, a metamodel summarising the look-up table is under construction. In order to identify the potential ecozones delimited by environmental scenarios, the next section provides an overview of potential changes to be expected across Europe for the next 30 years.

5.2 Scenarios of future forcings of European ecosystems.

In order to simulate atmospheric chemistry trajectories and climate, we worked in partnership with the CNRM-Meteo France (V. Marecal, B. Josse and K. Lamy), using the chemical transport model (CTM) MOCAGE (Josse et al., 2004, Teyssedre et al. 2007). This model was able to simulate the variables of interest at an hourly basis for the historical period 1995-2015 and for the 2015-2050 period with a spatial resolution of 0.5°×0.5° across Europe:

- Concentration (ppb) and wet/dry deposition of ozone O_3 (mol m^{-2} h^{-1}), (fig. 12).

- Concentration of nitrogen oxides (NOx as NO, NO_2 and NO_3)

- Nitrogen wet and dry deposition (NO_2 et NO_3)

MOCAGE uses climate projections from the ARPEGE-Climat GCM in its native global grid with a resolution of 0.5° over Europe. For the RINGO task 3.5 projections (2015-2050 period), the RCP4.5 climate scenario and the ECLIPSE anthropogenic emissions v4.a scenario for air pollutant emissions were used (http://eclipse.nilu.no/). The latter corresponds to the annual sums of emissions of different components following the Maximum Feasible Reduction (MFR) legislation. The EMEP data were also used for past reconstruction from 1996 to 2012 that serves to evaluate the model results and compare them with data. The fig. 12 shows the data simulated at the FR-Gri cropland site during summer 2005 together with the data observed in situ.

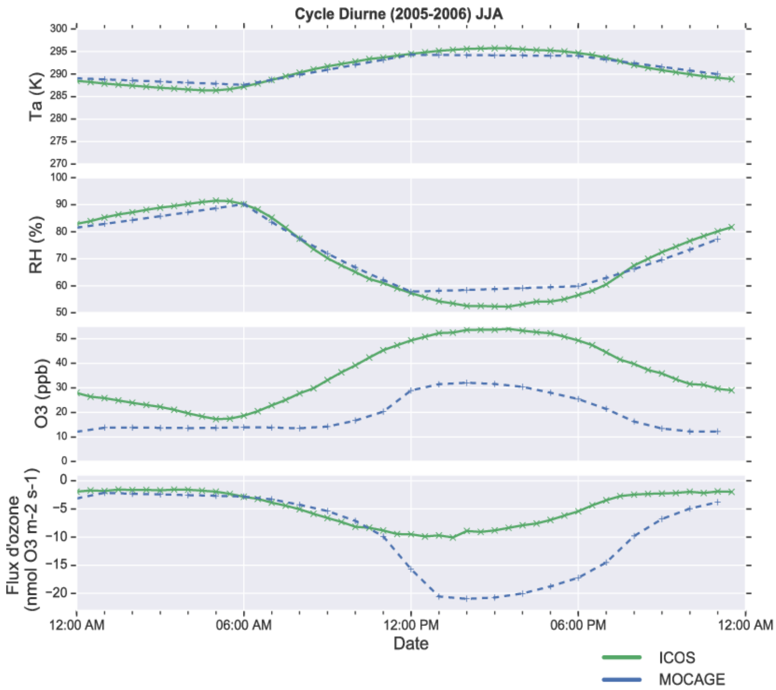

Figure 11. Mean daily cycle of air temperature and humidity, ozone concentration and deposition during the growing season (JJA) 2005 measured by the ICOS instruments and simulated by the MOCAGE model.

Time disaggregation to hourly scale was obtained from GENEMIS data (Ebel et al., 1994) using hourly coefficients depending on the activity sector (Society, 1994). The discrepancy shown in ozone data may be due to the resolution (0.5 x0.5°) of the MOCAGE results but were still surprising because previous comparisons showed better agreement with in situ measurements. The parameterisation of the deposition velocity might also explain the underestimate of MOCAGE results, the soil thickness being overestimated here which lead to overestimate the ozone deposition and underestimate the surface ozone concentration. Indeed, the mean bias observed with revised values of soil thickness (experiment 289) was close from null. The mean bias of the projections across Europe of simulated concentrations did not show marked spatial inhomogeneities. Almost in parallel with the RINGO project, Ducker et al. have reconstructed historical deposition rates over flux tower stations in US and Europe (Ducker et al. 2018)

The other drivers analysed are still being explored following the same approach. At this stage we think it is however appropriate to share this discussion with other *in situ* infrastructures in order to coordinate the interoperability of existing infrastructures and organise synergies and complementarity.

Reconstructed dry deposition of ozone across the ICOS ecosystem stations network

We consider the retrospective simulations of ozone deposition on pre-ICOS stations. The trend of stomatal ozone deposition in ICOS sites as modelled by MOCAGE and by the SYNFLUX model are presented below. The figure 12 illustrates how the concept of ecozone could be applied using the MOCAGE model and RCP 4.5 scenario.

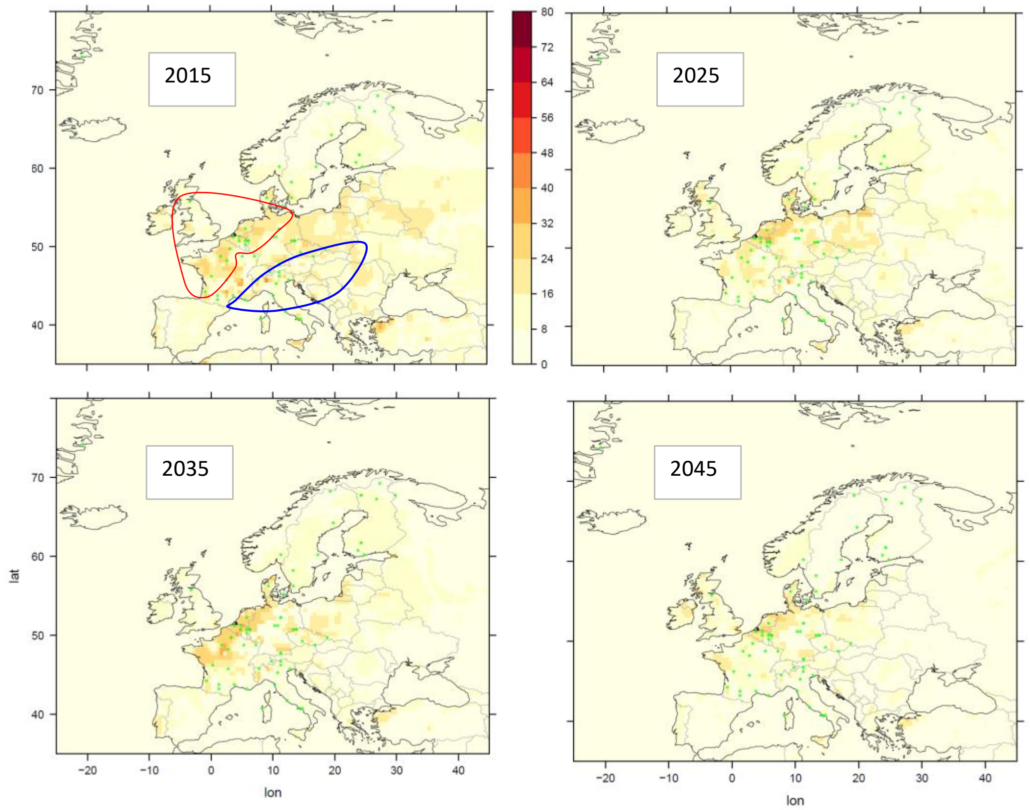

Figure 12. Projected dry deposition of Ozone across Europe (nmol m^{-2} s^{-1}). Average hourly values (at 4:00 pm during the growing season (JJA). Green dots are ecosystem stations registered in the ICOS-RI. Modelling by ARPEGE-ALADIN GCM / RCM and the CHIMERE chemistry – transport model under RCP4.5 scenario and ECLIPSE, MRF scenario. Green diamonds represent the 66 ICOS ecosystems stations. The red heart refers to the ecozone (1) for which O_3 dry deposition is a high in summer (10 stations) and has increased with time and whereas the blue ellipsoid refers to the ecozone (3) where O_3 dry deposition is more scattered and would significantly decrease with time (about 22 stations). Area outside the previous red and blue zones is ecozone (2) that shows no substantial change in O_3 deposition.

The future expected tendency across Europe allows to delimit three ecozones as three zones extending respectively (fig. 12):

- from NE-SW from the Channel and North Sea SW shore (Denmark, The Netherlands, Belgium , French Normandy, (ecozone 1, in red)
- the Scandinavia , centres of France and Germany (ecozone 2)
- the Alps and Northern Italy (ecozone 3, in blue).

The dry deposition rate of ozone is declining from EZ-1 to EZ-3 and EZ-2. Its shows a temporal decline until 2045, although 2035 levels exhibit a secondary peak in EZ-1. The reconstructions of ozone deposition by the MOCAGE and SYNFLUX models are consistent with the partitioning of the European area into 3 ecozones. The SYNFLUX simulations shown in fig. 13. are partitioned among the three ecozones EZ-1 to EZ-3 described above, and among PFTs. Although these data exhibit a substantial scattering, the figure shows the ozone deposition evolution has different patterns among ecozones and PFTs. Apart from the coniferous forests ENF of the EZ-3 (Alps and Italy), the highest deposition rates observed in early summer were generally observed in EZ-1 with a decreasing trend over time. Conversely, the deposition over the ENF type ecosystems in EZ-2 almost doubled from 2006 to 2015.

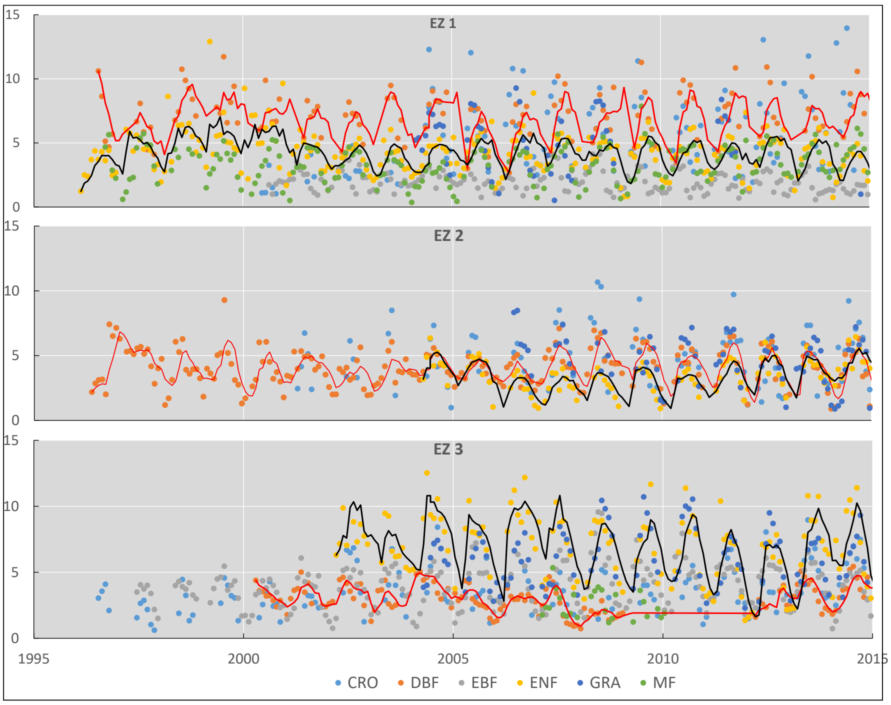

Figure 13. Reconstruction of ozone dry deposition over ecosystem sites monitored by the ICOS stations along the 1995-2015 period with the SYNFLUX model (Ducker et al. 2018). The ecosystems are split by PFT (IGPB classification). The coloured curves are moving averages for the broadleaved forests (DBF in red) and coniferous forests (ENF in black).

The figure 14 is a focus on simulated time series of Ozone dry deposition onto the French stations split among EZ-1 (FR-Gri, FR-Bil, FR-EM2, FR-Lus, Fr-Fon) and EZ-2 (FR-FBn, FR-Hes, FR-Aur, FR Lam). Two Finnish stations located in EZ-2 are also shown (FI-Var, FI-Sod). This figure also confirms the contrast between ecozones 1 and 2 but no clear temporal trend is revealed here (note that all the PFTs are pooled here). The stations located in EZ1 received through dry deposition twice the amount of ozone received by the stations located in EZ2.

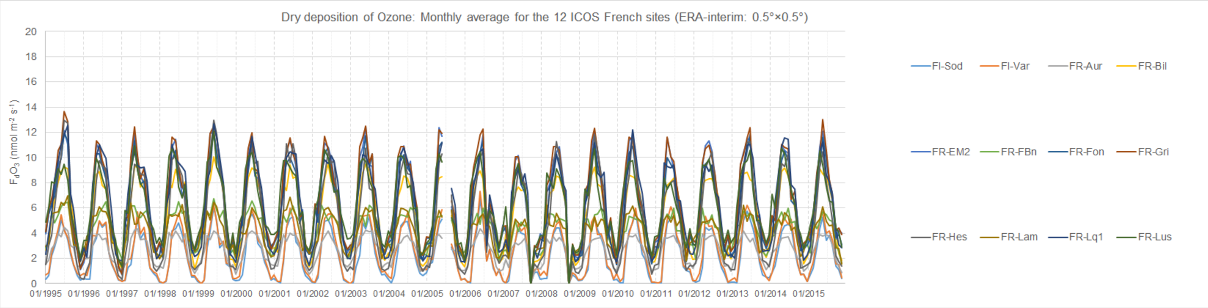

Figure 15. Time-series (1995-2015) of monthly average of hourly ozone dry depositions (nmol m-2 s-1) for 12 ICOS French sites simulated with MOCAGE.

This example shows that, in the future, the analysis of ecosystem data may benefit from clustering stations among ecozones and PFTs to evidence environmental impacts on continental ecosystems. In addition, the ecozone concept allows to substitute the space for time through synchronic comparison of stations exposed to e.g. contrasted level of pollution. Recent comparisons between urban and rural stations during the 2019 lock down period is supporting this approach (Fares, unpublished personal communication, 2020).

5.3. Optimising the sensitivity of in situ networks: a tentative roadmap

The look up table of network sensitivity and the ecozone concept developed above can support the optimisation of the Ecosystem stations network observing the ecosystems in situ. We also know from literature that, depending on the driver involved, the PFTs are not equally sensitive. Second, the selection of the target variables are key for evidencing environmental impacts. Here, with respect to the detection of past and future environmental impacts on ecosystems, we propose a general framework that may help to optimise the present ecosystem stations network devoted to *in situ* observations. Starting from the general measurement model (Eq. 1), the optimisation approach may concern the following network characteristics:

1. *Maximising the impact of drivers* (parameter *a*). The selection of appropriate "target" variables comes first. It must rely on the knowledge of potential impacts on ecosystems, their physiology and functioning. When cumulative, the impact to be observed increases with time, e.g. the atmospheric CO_2 concentration effect on GPP, so that the measurement duration plays obviously a key role: we showed that the CO_2 impact may not be observed in time series shorter than 10 to 15 years.

2. *Reducing the measurement uncertainty* (parameter ε). The variable selection and metrological practices may both contribute to minimise the uncertainty of the target variable. Variable with higher accuracy should of course be preferred for detecting a given impact. For instance, as shown with GPP_{max} vs GPP, instantaneous values of flux variables may have different errors than longer time integrals because they can be sampled repeatedly and have no gap filling errors. In addition, time series showing higher completeness have lesser gap-filling errors which strongly argues in favor of a high level of instrument and station maintenance. Reducing the measurement uncertainty must be based also upon methodological improvements and good metrological practices that must be applied to every station of the network.

3. *Minimising the background temporal variability (σ).* As far as the detection of temporal changes is concerned, the PFT are not all equivalent because ecosystems that are heavily manipulated such as crops and cultivated grasslands shows indeed a higher temporal variability. Conversely, ecosystems that includes long-lived vegetation with slow growth and no or light management are better suited for evidencing subtle environmental changes, i.e. the forests, natural grasslands, wetlands and shrublands. The clustering of stations within ecozones and the intercomparison of ecozones submitted to different levels of exposition allows to reduce the effect of the background variability. For instance comparing ecozones, such as neighbouring rural and urban stations, may allow to analyse the impact of environmental drivers, e.g. the ozone pollution effects, while attenuating the effects of other factors. In other words, comparing stations among ecozones is a way to analyse the time course of the difference among stations and detect putative anomalies due to a change in a driver in the exposed ecozone.

4. *Optimising the network design*. The look up table synthetizing the sensitivity of possible design of ecosystem stations provides a basis for calculating the gain in sensitivity to be expected from adding supplementary stations, lengthening the network duration and reducing the uncertainty. The figure 5 shows that the marginal gains are not linear and that the larger gain are estimated when increasing the network size and duration up to minimum threshold. There is also a substantial gain to obtain from improving metrological practices, this gain being larger for detecting subtle effects.
   We conclude that there is substantial gains in sensitivity to be expected from the networks of ecosystem stations spread over the European continent providing a minimum number of 10 stations of the different forest, wetlands and grasslands PFTS are operating for a minimum duration of 15 years in each of the main possible ecozones. As a first step we would therefore recommend to check:

   - the number of stations operating in each PFTs and climate zone and propose eventually to add supplementary stations;
   - their interoperability, metrological compatibility and data availability;
   - the completeness of the list of variables measured on site or nearby and ensure that potential target variables are monitored. In addition to the existing ICOS variables[2], some ecophysiological measurements to be operated on sample of trees such as xylem sap flow, transpiration, foliage temperature and stomatal conductance might be relevant in that respect. Other target variables concerning the plant, animal and microbe species diversity, plant traits and phenology are prone to rapid changes etc. must be added as well.
   - the environmental drivers involved in a visible future are all monitored and that the related data are available according to FAIR principles. This is particularly important but also challenging. If the temporal changes in ecosystem functioning have to be correctly attributed to causal factors, the biotic and abiotic drivers at work must be characterised. Such an appraisal is only feasible through a strong co-operation between existing infrastructures and must benefit from space-based observations.

The recommendations 1-4 provide a general framework for optimising in situ observations on European ecosystems. This optimisation is envisioned as a virtuous and continuous cycling

[2] http://gaia.agraria.unitus.it/icos/documents/Variables

process as shown below (fig. 15). Such a strategy goes well beyond the only ICOS Ecosystem infrastructure. It has to be shared with similar Ecosystem infrastructures such as ICOS-Atmospheric network, ELTER-RI, DANUBIUS-RI, ICP-Forests, ACTRIS-RI, and Copernicus programs. It was beyond the capability of the task 3.5 of the RINGO project to develop a complete inventory of stations and scenarios across infrastructures and for the entire Europe, check the list measurements in operation, data available and their interoperability. These will be partly some outcomes of the ENVRI-FAIR project. Our retrospective analysis, network model, and conclusions drawn provide rather a tentative conceptual basis for proposing an optimisation of the existing infrastructures in the next European framework, among the lines 1-4 developed above.

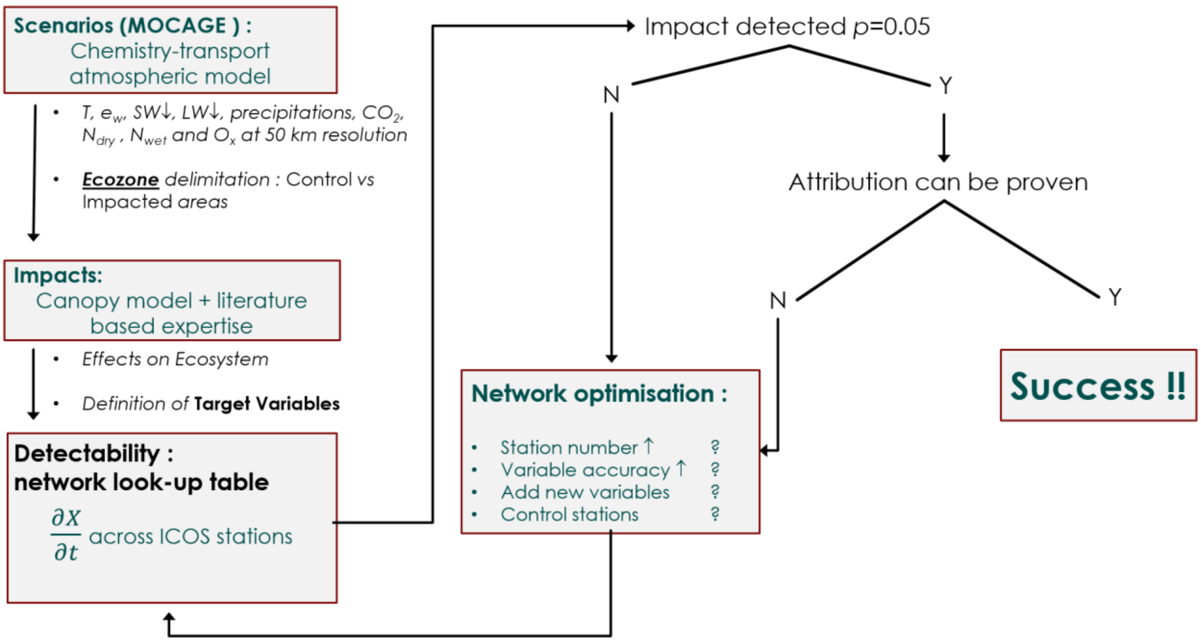

Figure 15. Optimisation scheme for improving the sensitivity of ecosystem observations to environmental changes and their attribution to the drivers involved.

Data used.

This work used eddy covariance data acquired and shared by the FLUXNET community, including these networks: AmeriFlux, AfriFlux, AsiaFlux, CarboAfrica, CarboEuropeIP, CarboItaly, CarboMont, ChinaFlux, Fluxnet-Canada, GreenGrass, ICOS, KoFlux, LBA, NECC, OzFlux-TERN, TCOS-Siberia, and USCCC. The ERA-Interim reanalysis data are provided by ECMWF and processed by LSCE. The FLUXNET eddy covariance data processing and harmonization was carried out by the European Fluxes Database Cluster, AmeriFlux Management Project, and Fluxdata project of FLUXNET, with the support of CDIAC and ICOS Ecosystem Thematic Center, and the OzFlux, ChinaFlux and AsiaFlux offices.

FLUXNET2015 dataset : http://fluxnet.fluxdata.org/data/fluxnet2015-dataset/

Abbreviations

ACTRIS	Aerosol, Clouds and Trace Gases Research Infrastructure
CRO	Croplands functional type
CTM	Chemistry transport model
DANUBIUS	European research infrastructure on River-Sea Systems (basin, delta and sea)
DT	"Day time" method for partitioning CO_2 fluxes
EC	Eddy covariance
ELTER	Long-Term Ecological Research in Europe
EMEP	European Monitoring and Evaluation Programme
ENF	Evergreen needle leaf forest functional type
EZ	Eco-Zone
FAIR	Findable Accessible Interoperable Reusable
FLUXNET	World wide Network of Flux tower
GCM	Global circulation model
GPP	Gross primary production (more often its annual integral in this report)
GPP_{max}	Annual maximal of half-hourly values of GPP
ICP-Forests	International Cooperative Program on Forests observation
JJA	June-July-August
LAI	Leaf Area Index
MF	Mixed Forest functional type
NEE	Net ecosystem exchange in CO_2
NEON	National Ecological Observatory Network
NT	Night-time method method for partitioning CO_2 fluxes
PFT	Plant Functional type
PPFD	Photosynthetic Photon Flux Density
QA/QC	Quality assessment / Quality control
RCP	Representative Concentration Pathway (used for climate scenario construction)
u*	friction velocity
VPD	Air water vapour saturation deficit

References

(RINGO project publications of the Task 3.5 are bold).

Baldocchi, D., Falge, E., Wilson, K., 2001. A spectral analysis of biosphere–atmosphere trace gas flux densities and meteorological variables across hour to multi-year time scales. Agric. For. Meteorol. 107, 1–27. https://doi.org/10.1016/S0168-1923(00)00228-8

Baldocchi, D., 2008. “Breathing” of the terrestrial biosphere: lessons learned from a global network of carbon dioxide flux measurement systems. Aust. J. Bot. 56, 1. https://doi.org/10.1071/BT07151

Baldocchi, D. 2014. Measuring fluxes of trace gases and energy between ecosystems and the atmosphere – the state and future of the eddy covariance method. Global Change Biology 20(12): 3600-3609.

Baldocchi B., Chu H., Reichstein M., 2018. Inter-annual variability of net and gross ecosystem carbon fluxes: A review. Agricultural and Forest Meteorology. 249, 520-533. https://doi.org/10.1016/j.agrformet.2017.05.015.

Billesbach, D. P. 2011: Estimating uncertainties in individual eddy covariance flux measurements: A comparison of methods and aproposed new method, Agr. Forest Meteorol., 151, 394–405.

Ciais, P., Loustau, D., Bosc, A., Ogée, J., Dufrêne, E., François, C., Viovy, N., and Delage, F. 2011. How will the production of French forests respond to climate change? An integrated analysis from site to country scale. In: Forests, carbon cycle and climate change, Loustau, D.(Ed.), Quae, Paris.

Ebel, A., Friedrich, R., Rodhe, H., 1994. Tropospheric Modelling and Emission Estimation: Generation of European Emission Data for Episodes (GENEMIS) Project. EUROTRAC Annual Report 1993, Part 5.

Falge, E., D. Baldocchi, R. Olson, P. Anthoni, M. Aubinet, C. Bernhofer, G. Burba, R. Ceulemans, R. Clement, H. Dolman, A. Granier, P. Gross, T. Grunwald, D. Hollinger, N. O. Jensen, G. Katul, P. Keronen, A. Kowalski, C. T. Lai, B. E. Law, T. Meyers, H. Moncrieff, E. Moors, J. W. Munger, K. Pilegaard, U. Rannik, C. Rebmann, A. Suyker, J. Tenhunen, K. Tu, S. Verma, T. Vesala, K. Wilson and S. Wofsy, 2001. Gap filling strategies for defensible annual sums of net ecosystem exchange. Agricultural and Forest Meteorology 107(1): 43-69.

Fernandez-Martinez, M., Vicca, S., Janssens, I. A., Ciais, P., Obersteiner, M., Bartrons, M., Sardans, J., Verger, A., Canadell, J. G., Chevallier, F., Wang, X., Bernhofer, C., Curtis, P. S., Gianelle, D., Gruwald, T., Heinesch, B., Ibrom, A., Knohl, A., Laurila, T., Law, B. E., Limousin, J. M., Longdoz, B., Loustau, D., Mammarella, I., Matteucci, G., Monson, R. K., Montagnani, L., Moors, E. J., Munger, J. W., Papale, D., Piao, S. L., and Penuelas, J.: Atmospheric deposition, CO_2, and change in the land carbon sink, Scientific Reports, 7, 2017.

Finkelstein, P. L., and P. F. Sims. 2001. Sampling error in eddy correlation flux measurements. Journal of Geophysical Research, 106: 3503-3509.

Goodrich, J. P., W. C. Oechel, B. Gioli, V. Moreaux, P. C. Murphy, G. Burba and D. Zona (2016). "Impact of different eddy covariance sensors, site set-up, and maintenance on the annual balance of CO2 and CH4 in the harsh Arctic environment." Agricultural and Forest Meteorology 228: 239-251.

Hill T., Chocholek M., Clement R., 2017. The case for increasing the statistical power of eddy-covariance ecosystem studies: why, where and how? Global Change Biol., 23, 2154-2165.

Hollinger, D. Y. and A. D. Richardson (2005). "Uncertainty in eddy covariance measurements and its application to physiological models." Tree Physiology 25(7): 873-885.

Horemans, J. A., I. A. Janssens, B. Gielen, M. Roland, G. Deckmyn, A. Verstraeten, J. Neirynck and R. Ceulemans, 2020. Weather, pollution and biotic factors drive net forest - atmosphere exchange of CO2 at different temporal scales in a temperate-zone mixed forest. Agricultural and Forest Meteorology 291: 108059.

Josse, B., Simon, P., Peuch, V.-H., 2004. Rn-222 global simulations with the multiscale CTM MOCAGE. Tellus 56B, 339e356.

Lasslop, G., M. Reichstein, D. Papale, A. D. Richardson, A. Arneth, A. Barr, P. Stoy And G. Wohlfahrt, 2010. Separation of net ecosystem exchange into assimilation and respiration using a light response curve approach: critical issues and global evaluation. Global Change Biology 16(1): 187-208.

Lenschow, D. H., Wulfmeyer, V., and Senff, C. 2000: Measuring Second- through Fourth-Order Moments in Noisy Data, Journal of Atmosphericand Oceanic Technology, 17, 1330–1347, https://doi.org/10.1175/1520-0426(2000)017<1330:MSTFOM>2.0.CO;2.

Loustau, D., Bosc, A., Colin, A., Ogee, J., Davi, H., Francois, C., Dufrene, E., Deque, M., Cloppet, E., Arrouays, D., Le Bas, C., Saby, N., Pignard, G., Hamza, N., Granier, A., Breda, N., Ciais, P., Viovy, N., and Delage, F.: Modeling climate change effects on the potential production of French plains forests at the sub-regional level, Tree Physiol, 25, 813-823, 2005.

Mauder, M., M. Cuntz, C. Drue, A. Graf, C. Rebmann, H. P. Schmid, M. Schmidt and R. Steinbrecher 2013. A strategy for quality and uncertainty assessment of long-term eddy-covariance measurements. Agricultural and Forest Meteorology 169: 122-135.

Mauder, M. and T. Foken, 2006. Impact of post-field data processing on eddy covariance flux estimates and energy balance closure. Meteorologische Zeitschrift 15(6): 597-609.

Mauder, M., T. Foken, R. Clement, J. A. Elbers, W. Eugster, T. Grunwald, B. Heusinkveld and O. Kolle 2008. Quality control of CarboEurope flux data - Part 2: Inter-comparison of eddy-covariance software. Biogeosciences 5(2): 451-462.

Mauder, M. and M. J. Zeeman, 2018. Field intercomparison of prevailing sonic anemometers. Atmospheric Measurement Techniques 11(1): 249-263.

Moncrieff, J.B., Malhi, Y., Leuning, R., 1996. The propagation of errors in long-term measurements of land-atmosphere fluxes of carbon and water. Global Change Biol. 2, 231-240.

Moreaux, V., Martel, S., Bosc, A., Picart, D., Achat, D., Moisy, C., Aussenac, R., Chipeaux, C., Bonnefond, J. M., Trichet, P., Vezy, R., Badeau, V., Longdoz, B., Granier, A., Roupsard, O., Nicolas, M., Pilegaard, K., Matteucci, G., Jolivet, C., Black, A. T., Picard, O., and Loustau, D. 2020 (a) Energy, water and carbon exchanges in managed forest ecosystems: description, sensitivity analysis and evaluation of the INRAE GO+ model, version 3.0, Geosci. Model Dev. Discuss., 2020, 1-55, 2020.

Moreaux, V., Longdoz, B., Berveiller, D., Delpierre, N., Dufrêne, E., Bonnefond, J.-M., Chipeaux, C., Joffre, R., Limousin, J.-M., Ourcival, J.-M., Klumpp, K., Darsonville, O., Brut, A., Tallec, T., Ceschia, E., Panthou, G., and Loustau, D. 2020 (b). Environmental control of land-atmosphere CO2 fluxes from temperate ecosystems: a statistical approach based on homogenized time series from five land-use types, Tellus B: Chemical and Physical Meteorology, 72, 1-25, 2020.

Papale, D., Reichstein, M., Aubinet, M., Canfora, E., Bernhofer, C., Kutsch, W., Longdoz, B., Rambal, S., Valentini, R., Vesala, T., Yakir, D., 2006. Towards a standardized processing of net ecosystem exchange measured with eddy covariance technique: algorithms and uncertainty estimation. Biogeosciences 3, 571-583.

Pastorello, G. many more cp-authors and Papale, D., 2020. The FLUXNET2015 dataset and the ONEFlux processing pipeline for eddy covariance data, Scientific Data, 7, 225, 2020.

Pilegaard, K., A. Ibrom, M. S. Courtney, P. Hummelshøj and N. O. Jensen, 2011. Increasing net CO2 uptake by a Danish beech forest during the period from 1996 to 2009. Agricultural and Forest Meteorology 151(7): 934-946.

Rebmann, C., M. Aubinet, H. Schmid, N. Arriga, M. Aurela, G. Burba, R. Clement, A. De Ligne, G. Fratini, B. Gielen, J. Grace, A. Graf, P. Gross, S. Haapanala, M. Herbst, L. Hortnagl, A. Ibrom, L. Joly, N. Kljun, O. Kolle, A. Kowalski, A. Lindroth, D. Loustau, I. Mammarella, M. Mauder, L. Merbold, S. Metzger, M. Molder, L. Montagnani, D. Papale, M. Pavelka, M. Peichl, M. Roland, P. Serrano-Ortiz, L. Siebicke, R. Steinbrecher, J. P. Tuovinen, T. Vesala, G. Wohlfahrt and D. Franz 2018. ICOS eddy covariance flux-station site setup: a review. International Agrophysics 32(4): 471-+.

Shao, C. L., J. Q. Chen, C. A. Stepien, H. S. Chu, Z. T. Ouyang, T. B. Bridgeman, K. P. Czajkowski, R. H. Becker and R. John (2015). "Diurnal to annual changes in latent, sensible heat, and CO2 fluxes over a Laurentian Great Lake: A case study in Western Lake Erie." Journal of Geophysical Research-Biogeosciences 120(8): 1587-1604.

Reichstein, M., Falge, E., Baldocchi, D., Papale, D., Aubinet, M., Berbigier, P., Bernhofer, C., Buchmann, N., Gilmanov, T., Granier, A., Grunwald, T., Havrankova, K., Ilvesniemi, H., Janous, D., Knohl, A., Laurila, T., Lohila, A., Loustau, D., Matteucci, G., Meyers, T., Miglietta, F., Ourcival, J.M., Pumpanen, J., Rambal, S., Rotenberg, E., Sanz, M., Tenhunen, J., Seufert, G., Vaccari, F., Vesala, T., Yakir, D., Valentini, R., 2005. On the separation of net ecosystem exchange into assimilation and ecosystem respiration: review and improved algorithm. Global Change Biol. 11, 1424-1439.

Richardson, A.D., Hollinger, D.Y., Burba, G.G., Davis, K.J., Flanagan, L.B., Katul, G.G., Munger, J.W., Ricciuto, D.M., Stoy, P.C., Suyker, A.E., Verma, S.B., Wofsy, S.C., 2006. A multi-site analysis of random error in tower-based measurements of carbon and energy fluxes. Agric. Forest Meteorol. 136, 1-18.

Salesky, S.T., Chamecki, M. & Dias, N.L. 2012. Estimating the Random Error in Eddy-Covariance Based Fluxes and Other Turbulence Statistics: The Filtering Method. Boundary-Layer Meteorol 144, 113–135. doi:10.1007/s10546-012-9710-0

Society, E.I., 1994. Generation of European Emission Data for Episodes (GENEMIS) Project. EUROTRAC annual report 1993, part 5. Technical report, EUROTRAC. Garmish- artenkirchen, Germany.

Stoy, P.C., Katul, G.G., Siqueira, M.B.S., Juang, J.-Y., McCarthy, H.R., and co-authors. 2005. Variability in net ecosystem exchange from hourly to inter-annual time scales at adjacent pine and hardwood forests: a wavelet analysis. Tree Physiol. 25, 887–902. https://doi.org/10.1093/treephys/25.7.887

Stoy, P.C., Richardson, A.D., Baldocchi, D.D., Katul, G.G., Stanovick, J., and co-authors. 2009. Biosphere-atmosphere exchange of CO2 in relation to climate: a cross-biome analysis across multiple time scales. Biogeosciences 6, 2297–2312. https://doi.org/10.5194/bg-6-2297-2009Teyssedre H. et al. 2007. A new tropospheric and stratospheric Chemistry and Transport

Model MOCAGE-Climat for multi-year studies: evaluation of the present-day climatology and sensitivity to surface processes. Atmos. Chem. Phys., 7, 5815-5860.

Teyssedre, H., M. Michou, H. L. Clark, B. Josse, F. Karcher, D. Olivie, V. H. Peuch, D. Saint-Martin, D. Cariolle, J. L. Attie, P. Nedelec, P. Ricaud, V. Thouret, R. J. Van Der A, A. Volz-Thomas and F. Cheroux, 2007. A new tropospheric and stratospheric Chemistry and Transport Model MOCAGE-Climat for multi-year studies: evaluation of the present-day climatology and sensitivity to surface processes. Atmospheric Chemistry and Physics 7(22): 5815-5860.

Wang, H. J., W. J. Riley and W. D. Collins, 2015. Statistical uncertainty of eddy covariance CO2 fluxes inferred using a residual bootstrap approach. Agricultural and Forest Meteorology 206: 163-171.

Wesely M.L., Hart R.L. (1985) Variability of Short Term Eddy-Correlation Estimates of Mass Exchange. In: Hutchison B.A., Hicks B.B. (eds) The Forest-Atmosphere Interaction. Springer, Dordrecht. https://doi.org/10.1007/978-94-009-5305-5_35

Wofsy, S.C., M. L. Goulden, and J. W. Munger. 1993. Net exchange of CO2 in a mid-latitude forest, Science, 260, 1314-1317.

Wutzler, T., A. Lucas-Moffat, M. Migliavacca, J. Knauer, K. Sickel, L. Sigut, O. Menzer and M. Reichstein 2018. Basic and extensible post-processing of eddy covariance flux data with REddyProc. Biogeosciences 15(16): 5015-5030.

Zaehle, S., et al. (2014). Evaluation of 11 terrestrial carbon–nitrogen cycle models against observations from two temperate Free-Air CO2 Enrichment studies. New Phytologist 202(3): 803-822.

- Communications related to the RINGO Task 3.5.

Loustau D., Moreaux M. 2020. Detecting together what you cannot see alone: the ICOS station network case. European Research Course on Atmospheres. Introductory keynote. Grenoble 13 Janvier 2020. CNRS- Université de Grenoble Alpes. 40pl

Moreaux V., G. Panthou, B. Josse, K. Lamy, G. Bert, D. Papale, D. Loustau. 2020. Can we see it? How in situ observation networks may detect environmental impacts on ecosystem biogeochemistry. ICOS international Conference, Utrecht, 15-17 September 2020. Oral communication and poster.

Moreaux V., Gielen B., Papale D., Loustau. 2019. Optimising observation networks for the early detection and unequivocal attribution of environmental effects on European forests. IUFRO International Congress, Curitiba, Brazil, 29 sept. 5th Oct 2019. 20 pl. https://www.iufro.org/fileadmin/material/events/iwc19/iwc19-abstracts.pdf

Moreaux V. , Gielen B., Papale D., Loustau D. 2019. Enabling the observation networks of European Ecosystems to see the unseen: The sentinel network concept. ICOS 8th General Assembly – information day. 21st May, Saclay, France.

Appendix.

Appendix. 1.

Table A1. Lists of the sites in FLUXNET2015 database

site_id	PFT	site_id	PFT	site_id	PFT	site_id	PFT
AR-SLu	MF	BR-Sa3	EBF	CN-Sw2	GRA	FI-Let	ENF
AR-Vir	ENF	CA-Man	ENF	CZ-BK1	ENF	FI-Lom	WET
AT-Neu	GRA	CA-NS1	ENF	CZ-BK2	GRA	FI-Sod	ENF
AU-Ade	WSA	CA-NS2	ENF	CZ-wet	WET	FR-Fon	DBF
AU-ASM	ENF	CA-NS3	ENF	DE-Akm	WET	FR-Gri	CRO
AU-Cpr	SAV	CA-NS4	ENF	DE-Geb	CRO	FR-LBr	ENF
AU-Cum	EBF	CA-NS5	ENF	DE-Gri	GRA	FR-Pue	EBF
AU-DaP	GRA	CA-NS6	OSH	DE-Hai	DBF	GF-Guy	EBF
AU-DaS	SAV	CA-NS7	OSH	DE-Kli	CRO	IT-BCi	CRO
AU-Dry	SAV	CA-Qfo	ENF	DE-Lkb	ENF	IT-CA1	DBF
AU-Emr	GRA	CA-SF1	ENF	DE-Obe	ENF	IT-CA2	CRO
AU-Fog	WET	CA-SF2	ENF	DE-RuR	GRA	IT-CA3	DBF
AU-Gin	WSA	CA-SF3	OSH	DE-RuS	CRO	IT-Col	DBF
AU-How	WSA	CH-Cha	GRA	DE-Seh	CRO	IT-Cp2	EBF
AU-RDF	WSA	CH-Dav	ENF	DE-SfN	WET	IT-Cpz	EBF
AU-Rig	GRA	CH-Fru	GRA	DE-Spw	WET	IT-La2	ENF
AU-Stp	GRA	CH-Lae	MF	DE-Tha	ENF	IT-Lav	ENF
AU-Tum	EBF	CH-Oe1	GRA	DK-Eng	GRA	IT-MBo	GRA
AU-Wac	EBF	CH-Oe2	CRO	DK-NuF	WET	IT-Noe	CSH
AU-Whr	EBF	CN-Cha	MF	DK-Sor	DBF	IT-PT1	DBF
AU-Wom	EBF	CN-Cng	GRA	DK-ZaF	WET	IT-Ren	ENF
AU-Ync	GRA	CN-Din	EBF	DK-ZaH	GRA	IT-Ro1	DBF
BE-Bra	MF	CN-Du2	GRA	ES-LgS	OSH	IT-Ro2	DBF
BE-Lon	CRO	CN-Ha2	WET	ES-LJu	OSH	IT-SRo	ENF
BE-Vie	MF	CN-HaM	GRA	FI-Hyy	ENF	IT-Tor	GRA
JP-SMF	MF	CN-Qia	ENF	FI-Jok	CRO	JP-MBF	DBF
NL-Hor	GRA	US-ARM	CRO	US-Myb	WET	US-Twt	CRO

Table A1. Lists of the sites in FLUXNET2015 database (continued)

site_id	PFT	site_id	PFT	site_id	PFT	site_id	PFT
NL-Loo	ENF	US-Blo	ENF	US-Ne1	CRO	US-UMB	DBF
NO-Adv	WET	US-Cop	GRA	US-Ne2	CRO	US-UMd	DBF
RU-Che	WET	US-GBT	ENF	US-Ne3	CRO	US-Var	GRA
RU-Cok	OSH	US-GLE	ENF	US-NR1	ENF	US-WCr	DBF
RU-Fyo	ENF	US-Ha1	DBF	US-PFa	MF	US-Whs	OSH
RU-Ha1	GRA	US-KS2	CSH	US-Prr	ENF	US-Wi3	DBF
SD-Dem	SAV	US-Los	WET	US-SRC	MF	US-Wi4	ENF
SN-Dhr	SAV	US-Me2	ENF	US-SRM	WSA	US-Wkg	GRA
US-AR1	GRA	US-Me6	ENF	US-Syv	MF	ZA-Kru	SAV
US-AR2	GRA	US-MMS	DBF	US-Ton	WSA	ZM-Mon	DBF

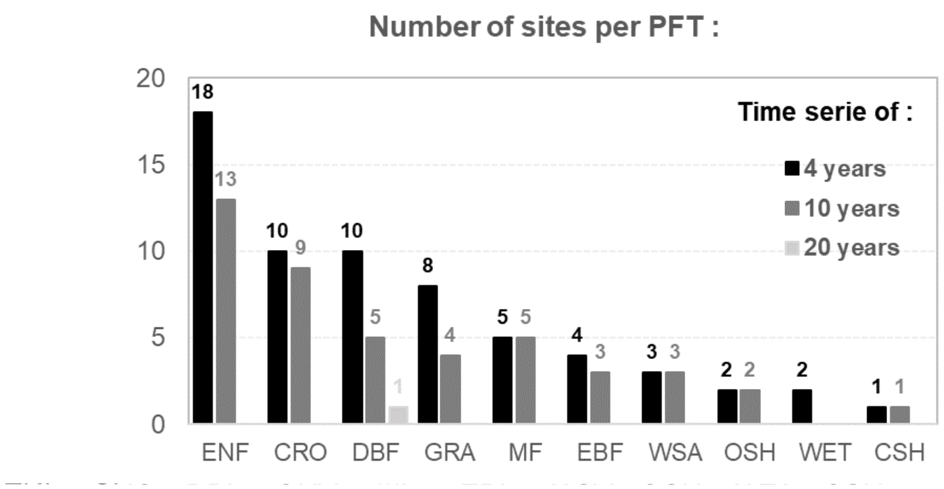

Figure A1. Number of ecosystem stations of the Fluxnet 2015 data set providing flux data from 1991 to 2014 and for three durations. Stations are pooled by PFT.

Appendix 2.

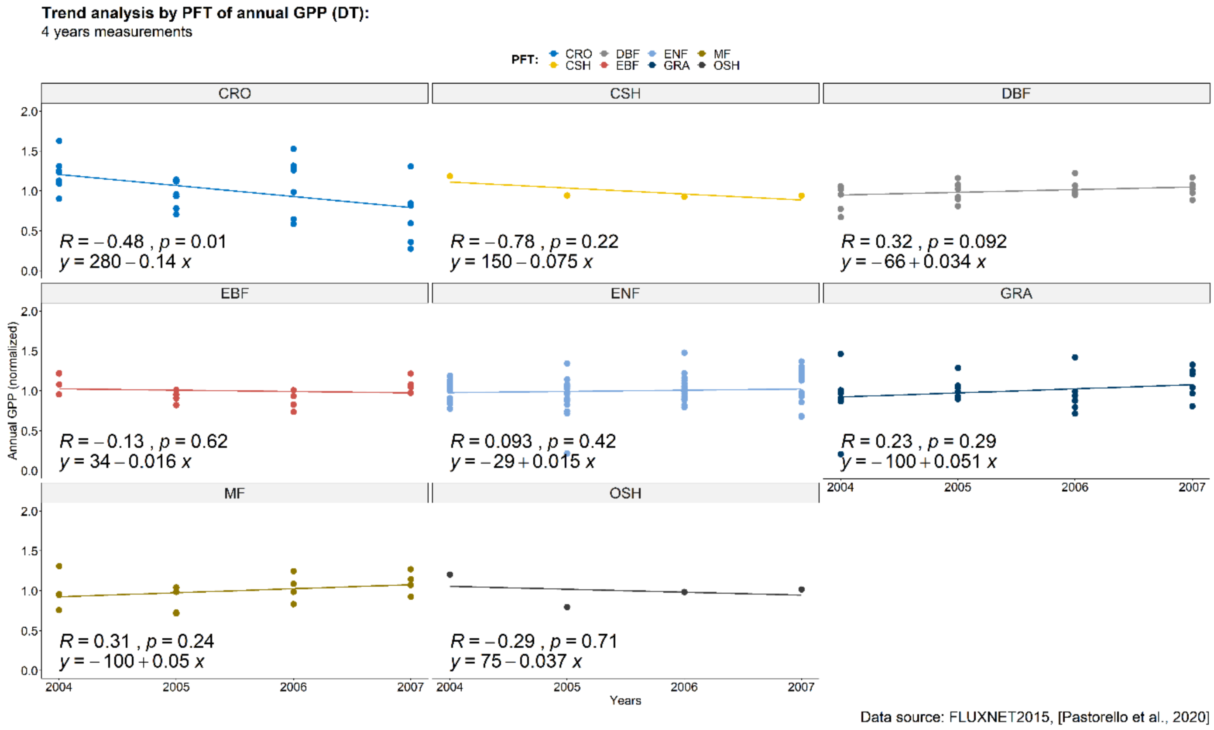

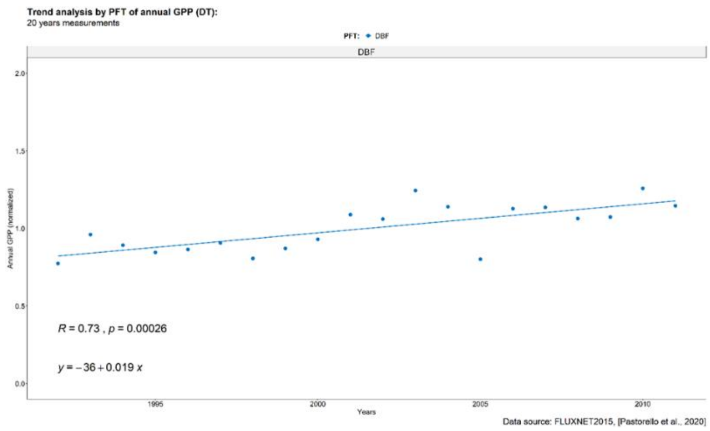

Figure A2. Linear regression of GPP over time by PFT for 4 year- (above diagrams) and 21-year (below diagram) long time series.

Appendix 3.

Table A2. Stations of the FLUXNET2015 database used for calculating the GPPmax time series

2004-2007		2004-2013		1996-2013		2004-2007 (continued)	
BE-Lon	CRO	BE-Lon	CRO	DK-Sor	DBF	IT-SRo	ENF
CH-Oe2	CRO	CH-Oe2	CRO	IT-Col	DBF	NL-Loo	ENF
DE-Geb	CRO	DE-Geb	CRO	DE-Tha	ENF	RU-Fyo	ENF
DE-Kli	CRO	DE-Kli	CRO	FI-Hyy	ENF	US-Blo	ENF
FR-Gri	CRO	FR-Gri	CRO	NL-Loo	ENF	US-Me2	ENF
IT-BCi	CRO	IT-BCi	CRO	BE-Vie	MF	US-Me3	ENF
US-ARM	CRO	IT-Noe	CSH			US-NR1	ENF
IT-Noe	CSH	DK-Sor	DBF			AT-Neu	GRA
CA-Oas	DBF	IT-Col	DBF			CH-Oe1	GRA
DE-Hai	DBF	US-Oho	DBF			DE-Gri	GRA
DK-Sor	DBF	FR-Pue	EBF			IT-MBo	GRA
IT-Col	DBF	GF-Guy	EBF			NL-Hor	GRA
IT-Ro1	DBF	CA-TP1	ENF			US-IB2	GRA
IT-Ro2	DBF	CA-TP3	ENF			BE-Bra	MF
US-Oho	DBF	CA-TP4	ENF			BE-Vie	MF
FR-Pue	EBF	CH-Dav	ENF			CA-Gro	MF
GF-Guy	EBF	CZ-BK1	ENF			CH-Lae	MF
IT-Cpz	EBF	DE-Tha	ENF			ES-LJu	OSH
MY-PSO	EBF	FI-Hyy	ENF				
CA-Obs	ENF	IT-Lav	ENF				
CA-Qfo	ENF	NL-Loo	ENF				
CA-TP1	ENF	RU-Fyo	ENF				
CA-TP2	ENF	US-Me2	ENF				
CA-TP3	ENF	US-NR1	ENF				
CA-TP4	ENF	DE-Gri	GRA				
CH-Dav	ENF	IT-MBo	GRA				
CZ-BK1	ENF	BE-Bra	MF				
DE-Tha	ENF	BE-Vie	MF				
FI-Hyy	ENF	CA-Gro	MF				
FR-LBr	ENF	CH-Lae	MF				
IT-Lav	ENF	ES-LJu	OSH				

Appendix 4.

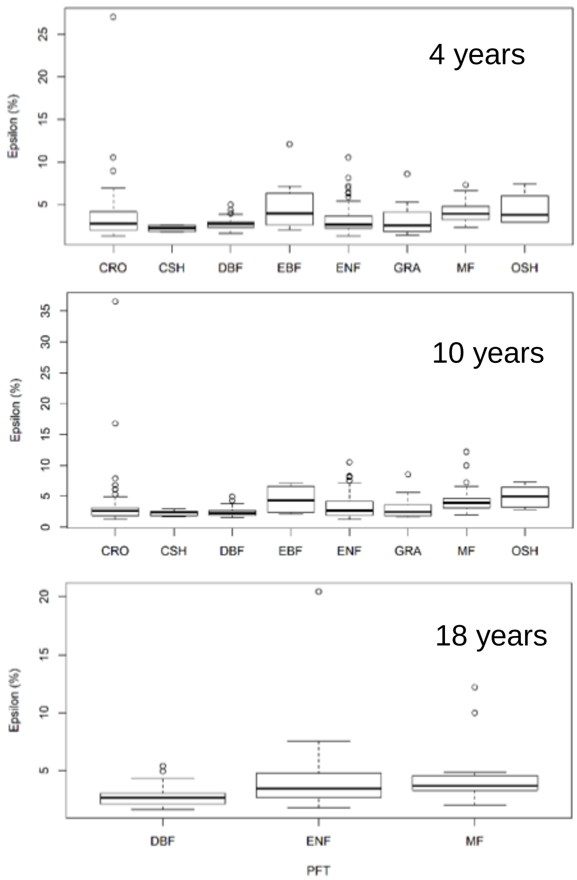

Figure A3. Error on GPPmax values by PFT calculated from 4, 10 and 18 year-long time series. Note the y axis scale is changed among plots.

Appendix 5.

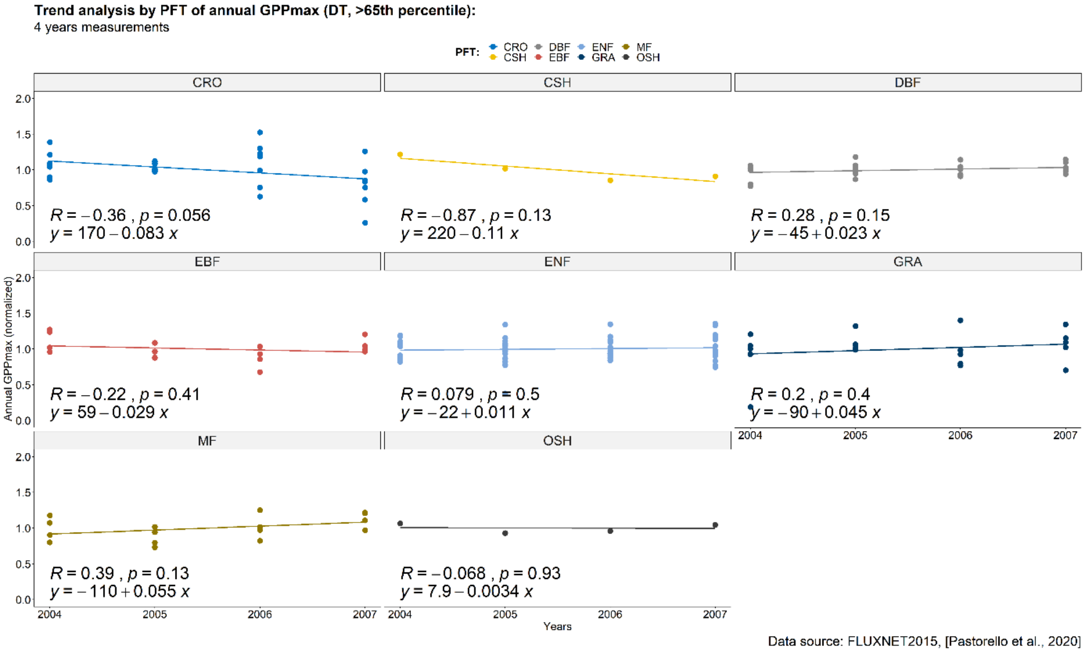

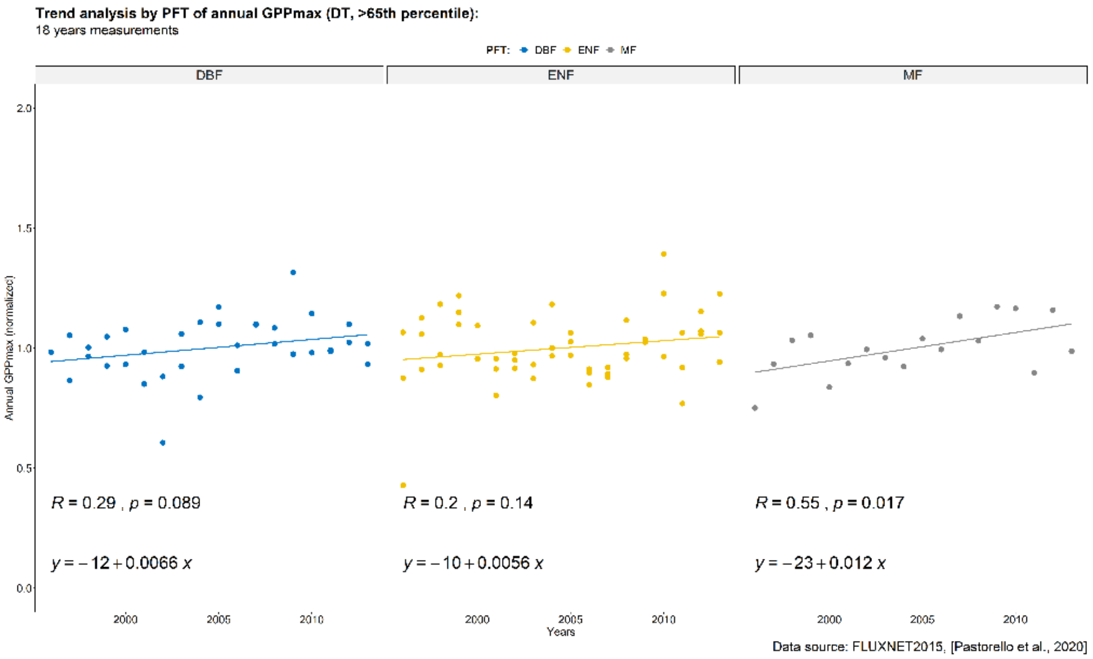

Figure A4. Linear regression of GPPmax over time by PFT along 4 year – and 18 year-long time series.